



Article

Achieving Sustainability and Cost-Effectiveness in Power Generation: Multi-Objective Dispatch of Solar, Wind, and Hydro Units

Mohammad Lotfi Akbarabadi ¹  and Reza Sirjani ^{2,*} 

¹ Department of Electrical and Electronic Engineering, Eastern Mediterranean University, Gazimagusa 99628, Turkey

² Department of Engineering and Physics, Karlstad University, 65188 Karlstad, Sweden

* Correspondence: reza.sirjani@kau.se

Abstract: In the power system, economic power dispatch is a popular and fundamental optimization problem. In its classical form, this problem only considers thermal generators and does not take into account network security constraints. However, other forms of the problem, such as economic emission dispatch (EED), are becoming increasingly important due to the emphasis on minimizing emissions for environmental purposes. The integration of renewable sources, such as solar, wind, and hydro units, is an important aspect of EED, but it can be challenging due to the stochastic nature of these sources. In this study, a multi-objective algorithm is developed to address the problem of economic emission power dispatch with the inclusion of these renewable sources. To account for the intermittent behavior of solar, wind, and hydro power, the algorithm uses Lognormal, Weibull, and Gumbel distributions, respectively. The algorithm also considers voltage limitations, transmission line capacities, prohibited areas of operation for thermal generator plants, and system restrictions. The multi-objective real coded non-dominated sorting genetic algorithm II (R-NSGA-II) is applied to the problem and includes a procedure for handling system restrictions to meet system limitations. Results are extracted using fuzzy decision-making and are analyzed and discussed. The proposed method is compared to other newer techniques from another study to demonstrate its robustness. The results show that the proposed method despite being older is cost-significant while maintaining the same or lower emissions. These results were observed consistently and did not happen by chance, detailed explanation of why and how is discussed.

Keywords: economic environmental dispatch; multi-objective optimization; renewable energy sources; stochastic modeling; fuzzy decision making; electrical power systems



Citation: Lotfi Akbarabadi, M.; Sirjani, R. Achieving Sustainability and Cost-Effectiveness in Power Generation: Multi-Objective Dispatch of Solar, Wind, and Hydro Units. *Sustainability* **2023**, *15*, 2407. <https://doi.org/10.3390/su15032407>

Academic Editors: Andreas Theocharis, Panos Kotsampopoulos and Grigorios L. Kyriakopoulos

Received: 31 October 2022
Revised: 13 January 2023
Accepted: 20 January 2023
Published: 29 January 2023



Copyright: © 2023 by the authors. Licensee MDPI, Basel, Switzerland. This article is an open access article distributed under the terms and conditions of the Creative Commons Attribution (CC BY) license (<https://creativecommons.org/licenses/by/4.0/>).

1. Introduction

Environmental concerns like global warming are becoming more eminent each day. Means of diminishing carbon emissions are the objectives of industries and governments, as they are trying to find techniques for solving this problem. Coal-powered units or central steam are getting old since distributed generation is the trend and motivation towards it is increasing. Penetration of different renewable sources can be enabled by a distributed generation where the location of consumers is closer to these sources of renewable energy [1]. Nevertheless, implementing renewable generation has its downsides and comes with different challenges.

Lasseter [2] introduced the microgrids concept as a way of implementing dispersed energy resources in a supervised and safe manner. A group of interlinked distributed energy resources and loads within distinctly established electrical borderlines that performs as an individual tractable unit vis-a-vis the grid is often defined as a microgrid. Operation of a microgrid can have two cases of grid-connected or islanded-mode since they can connect to the grid or disconnect from it to enable this feature. High penetration of different renewable

energy sources adds to the instability of the system because of the stochastic nature of them. Having implemented more than one class of renewable energy source like wind, solar or hydro will increase the uncertainty of the system even more. Since prediction error is the main relation of these uncertainties, reducing the instability of the network is important and can be achieved by studying different scenarios for each renewable type that exists within the system.

Economic Dispatch (ED) is the determination of the minimum possible cost for the required power from each committed power plant. In ED, there is usually one objective to be focused on: cost. The main objective in optimizing an ED problem is to reduce the total cost of generation as much as possible, to have an economic dispatch as the name suggests. In economic emission dispatch (EED), the main objective is to minimize the total price of generation as well as the emission degree. In both ED and EED, fulfilling electricity demand from the power units must be satisfied. Usually, the difference between ED and EED is that the former is a single-objective problem while the latter is a multi-objective problem. In EED one objective is to reduce emissions, and climatic contamination is mostly caused by thermal power units which produce Sulphur dioxide, a toxic gas, represented by SO_2 , and other similar gases like Nitrogen oxide and Carbon dioxide represented by NO_x and CO_2 , respectively [3]. There can be three different ways of solving EED according to Refs. [3–5]. Firstly, the problem is considered to be a single objective, only containing emissions, since in many countries environmental laws impose a carbon tax, hence practicing emission control is of more importance. This approach of reducing emissions at any cost is not an ideal solution and it should not be called EED anymore since there would not be a concern to reduce cost. The second way is to mix emission and cost into a single objective optimization and reduce them at the same time by considering different weights, and thirdly, with multi-objective optimization which has different and separate functions, in this case, cost and emission.

A solution to the EED problem falls into the two parts of economic dispatch and emission optimization. In the first part, optimal scheduling of generator units is performed to reduce electricity demand while in the second part, the same task is performed to diminish the number of harmful gases. Furthermore, an optimization method is needed to compute the optimal output for EED since there can be too many numbers of generation units in the system to be enumerated one by one. Diminishing cost or emission alone is also a single objective problem but reducing both of them at the same time, makes the problem very non-convex. Hence, there is more than one solution to the problem and specific methods must be used to extract those answers for a trade-off between emission and cost. This means that by reducing emissions, the cost will increase and vice versa. In the following paragraphs, previous studies that solved ED and EED problems will be mentioned. Their optimization technique will be reviewed and we will point out what renewable energy source was incorporated and what consideration has been taken into account for system limitations.

Adarsh et al. [6] solved ED by chaotic bat algorithm, a variant of swarm intelligence technique combined with chaotic sequences for tuning and controlling the parameters resulting in convergence and diversity enhancement. Jayabarathi et al. [7] implemented the hybrid gray wolf algorithm to solve the ED problem. They acquired genetic operators (crossover and mutation) for enhancing the algorithms' performance and they also considered prohibited operating zones (POZs), and valve point effect, but they did not consider a multi-fuel option. The introduction of the multi-fuel option was performed in Ref. [8], and they used crisscross optimization to solve the ED problem but without considering POZs. Delshad et al. [9] utilized a backtracking search algorithm (BSA) containing various feed options and valve-point effects. They added more complexity to the ED problem by considering POZs, and generators ramp-up and ramp-down since BSA is promoted to solve very non-convex functions. Even though their formulation for the ED problem was good, it lacked consideration of reducing emissions.

Implementing emission into the formula requires multi-objective optimization. Di Somma et al. [10] used a stochastic multi-objective optimization to reduce the cost and emission and prioritized environmental aspects with a focus on optimal scheduling. Secui [11] used an approach known as the weighted sum, with a newly altered artificial bee colony algorithm to approach the ED problem. Aside from the valve-point effect, other restrictions like transmission losses, POZ, and ramp-rate boundaries have been considered to improve the mathematical model. However, no renewable energy sources were considered in the formulation of the problem. Ghasemi et al. [12] considered wind units in their formulation and they implemented a 2m-point practical model for the uncertainty in wind power. This was a multi-objective economic emission dispatch (MOEED) problem and they solved it by using the honey bee mating optimization technique. However, they compared the results with very old optimization methods that have poor constraint-handling techniques. Qu et al. [13] used the summation-based differential evolution technique in a multi-objective form and considered the uncertainty of wind to be a limitation of the system while applying the superiority of a feasible solution as a constraint-handling method. Only the implementation of the wind plant was considered up to this point. Khan et al. [14] solved EED with thermal and solar power by applying the particle swarm method while converting the multi-objective function to a single-objective function. This can hurt the performance of the optimization since a trade-off must happen between cost and emission. Kheshti et al. [15] introduced Lightning Flash Algorithm. A new evolutionary algorithm for solving non-convex large-scale EED problems considering valve-point effects and multiple fuel options. However, they did not consider any wind plant in their problem formulation. Not too much literature can be traced regarding the model of solar, thermal, and wind plant in power systems and this is true for a combination of wind and hydro energy sources. Hence, more research is required.

Reddy et al. [16] considered wind, thermal and solar power in the system and approached the scheduling problem with the best-fit evaluation of participation factors. However, they performed single objective optimization of the system and did not consider emission reduction. Reddy [17] executed optimal scheduling of a hybrid system (wind-solar-thermal) together by using a two-point estimate method and genetic algorithm. To consider emission reduction, battery storage was proposed but this still is a single objective problem. Biswas et al. [18] used the success history-based adaptation technique to solve the optimal flow problem incorporated with solar and wind plants. However, the problem formulation was a single objective problem but they used separate probability density functions to estimate the stochastic behavior of renewable energy sources as well as the underestimation and overestimation price of them. Liu et al. [19] integrated the improved gradient descent with an evolutionary algorithm to solve the dynamic economic dispatch problem containing small hydro and wind energy sources. Gumbel and Weibull probability density functions were used to represent the random behavior of the mentioned energy sources, respectively. Up to here, no multi-objective optimization was performed for EED.

Salkuti [20] computed single and multi-objective EED problems by adding thermal-wind-solar power in the system and implemented prohibited operating zones and valve point loading effect but he did not use a proper constrain handling technique and the optimization algorithm (particle swarm optimization) was too old. Yalcinoz et al. [21] used improved particle swarm optimization to solve the MOEED problem while implementing wind energy in the system and considering generator limitations, valve point effect, ramp restrictions, transmission losses, and prohibited operating zones. Nevertheless, they did not consider a proper constraint-handling method nor an appropriate decision-making solution for optimization results. When the problem requires multi-objective optimization, a method of extracting compromised solutions is needed. It is important to take into account how the decision-making of extracting results is going to take place. Decision-making methods that can consider multiple objectives at the same time are needed in order to create energy planning scenarios that take into account social, economic, environmental, and technical aspects related to human development [22].

Renewable energy sources like wind and solar can fluctuate randomly, which makes it risky for a single unit to participate in the energy market. If the unit is unable to produce power, purchasing power at a high price from the balancing markets is needed [23], and this shows the importance of implementing different renewable energy units in the system. Until here, a combination of wind, small-hydro, solar, and thermal power plants has not been mentioned and many of these articles did not consider a proper constraint handling technique nor a proper technique to extract the compromised solution. To the best of our knowledge combination of these energy sources altogether, considering different aspects of system limitations while taking into account different probability density functions for predicting the stochastic behavior of renewables has been demonstrated only in Ref. [24].

In this study, we considered many system limitations such as generator limits, POZs, valve point effects, network security, etc. while performing MOEED with thermal generators, the solar, wind, and hydro renewable sources. In this approach, we also considered a proper constraint-handling method and emphasized the importance of carefully selecting different optimization parameters. This study aims to:

1. Contemplate forecasting of renewable energy sources of different types and their implementation in the system.
2. Formulate and demonstrate a solution to MOEED that is a very non-convex and non-linear problem.
3. Give in-depth knowledge of optimization since developing an algorithm that is reliable, fast, robust, and able to handle multi-objective optimization requires a deep understanding of the underlying principles and techniques.
4. Satisfy many system constraints and network securities that go beyond the classical approach by using a proper constraint-handling method.
5. Analyze the results in detail and compare them with previous studies to assess the robustness, stability, and quality of this strategy.

This paper is categorized in the following manner. In Section 1, we begin with an introduction to the problem and its significance, highlighting the research background and outlining the main objectives of this study. We then delve deeper into the topic with a thorough literature review, discussing the latest developments and trends in this area. Different methods of optimization are reviewed and key concepts and ideas behind the problem formulation are stated. The limitations of previous articles are mentioned. Section 2 formally presents the detailed methodology that is practiced in this study. It states the proposed R-NSGA-II and its elitist characteristics alongside the genetic operators that are carefully selected and incorporated within. It also includes an explanation of different methods which are used to forecast renewable energy sources and their implementation in the modified IEEE 30 bus system. Furthermore, it provides methods of extracting the best-compromised solution integrated with the algorithm. It talks about a proper and strong constraint-handling technique. Section 3 presents the outcomes of the simulation for the developed algorithm on the modified IEEE 30 bus network combined with renewable energy sources. It also shows the compared results with two other algorithms (which are newer and supposed to be better) to assess the accomplishments of the suggested approach. Section 4 summarizes and concludes the presented study. It suggests possible future work that can be implemented and studied, and the limitations of this study.

2. Materials and Methods

2.1. Specification of the System

The main characteristics of the adjusted IEEE 30-bus network [24] can be seen in Table 1. The revised network's illustration can be seen in Figure 1. The system has 30 buses and 41 branches. Three thermal generators are connected to the system, one generator at bus number 1, another generator at bus 2, and the last generator at bus 8. A wind generator is supplying bus 5. A solar photovoltaic (SPV) plant is at bus 11. A solar unit combined with a small-hydro plant is at bus 13. We have 11 control variables (inputs) in the system. The scheduled real power of five generators is indicated by T_{G2} , T_{G3} , W_G , PV , and PVH ; bus

voltage of all six plants. All these 11 control variables should be optimized thus maintaining the economical and efficient operation of the system.

Table 1. Essential features of the revised IEEE 30-bus system [24].

Specific Characteristics	Amount	Details
Corresponding load (P and Q)	-	283.4 MW, 126.2 MVar
Acceptable load bus voltage range	24	0.95–1.10 (p.u.)

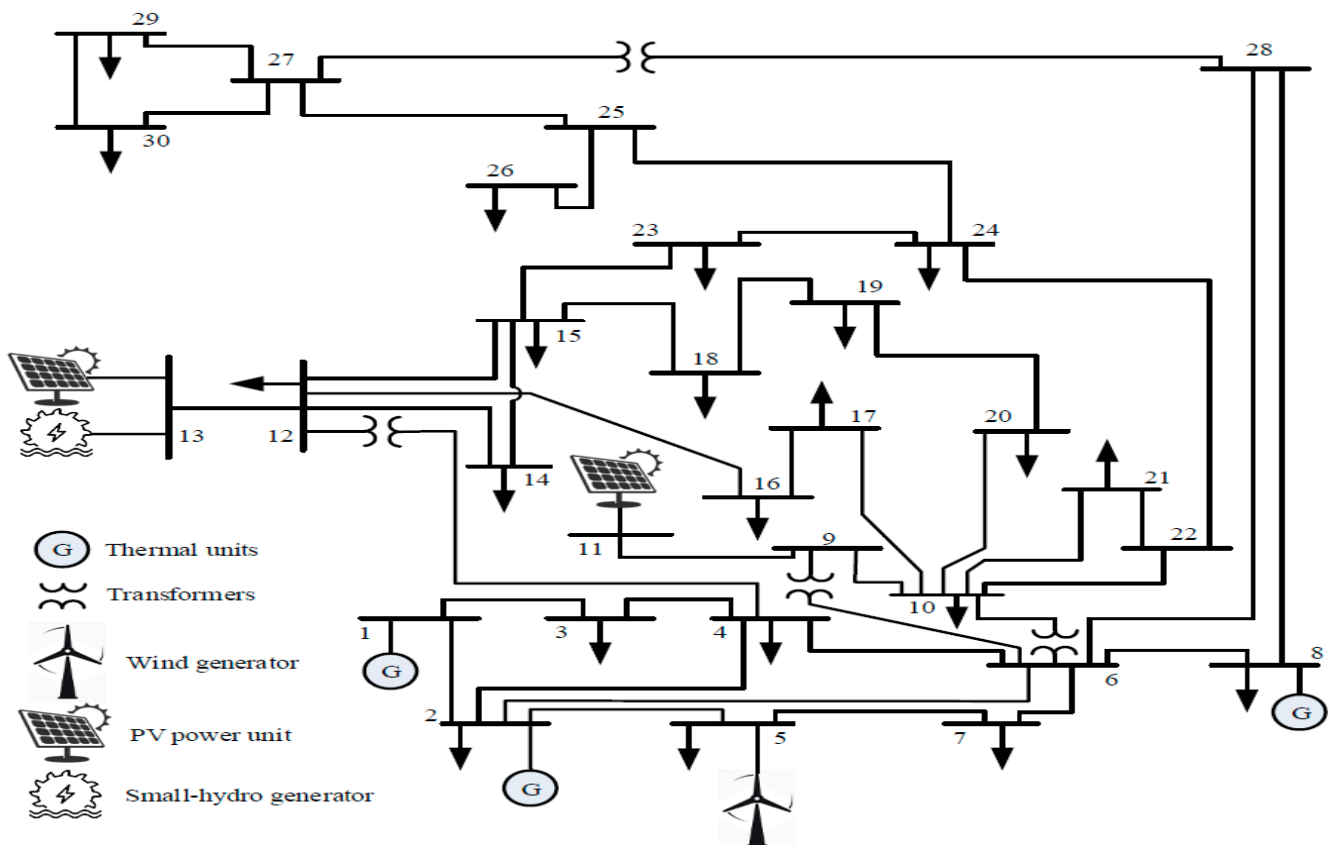


Figure 1. The revised IEEE structure with 30 buses having solar, small hydro, and wind plants [24].

A run-of-river small-hydro power unit is considered so that there would be no need for storage in most cases. A small-hydro has the potential of giving a few megawatts as output power at best [25]. There comes the SPV unit, which is integrated with the small-hydro unit supplying bus 13 to improve the total output power. It is obvious that the outputs of a solar plant, wind, and small-hydro units are variable dependent and any amount of output shortage from them must be diminished by the spinning reserve.

2.2. Thermal Generator Cost

Fuel price (in \$/h) for the thermal plant complies with a quadratic curve that can be expressed as [18]:

$$C_{T0}(P_{TG}) = \sum_{i=1}^{N_{TG}} a_i + b_i P_{TG_i} + c_i P_{TG_i}^2 \quad (1)$$

where a_i , b_i , and c_i show the price coefficients of the i^{th} thermal plant P_{TG_i} . N_{TG} is the entire number of thermal plants in the system. The cost function for a generator is not smooth due to the valve point loading effect [26]. By considering the valve-point loading effect, due to the presence of stacking impacts of the valve point, the generation fuel cost function grows into non-convex with so many curls and it can be seen in Figure 2. To be

more accurate, the increased charge due to the effects of steam, i.e., valve-point is treated as [18]:

$$C_T(P_{TG}) = \sum_{i=1}^{N_{TG}} a_i + b_i P_{TGi} + c_i P_{TGi}^2 + \left| d_i \times \sin \left(e_i \times (P_{TGi}^{\min} - P_{TGi}) \right) \right| \quad (2)$$

where e_i and d_i are for considering the price coefficients of the valve-point effect. The lowest output of the i^{th} thermal plant when it is operating is P_{TGi}^{\min} . The price coefficients of thermal generator plants are provided in Table 2. The explanation for some symbols can be found in Equation (12).

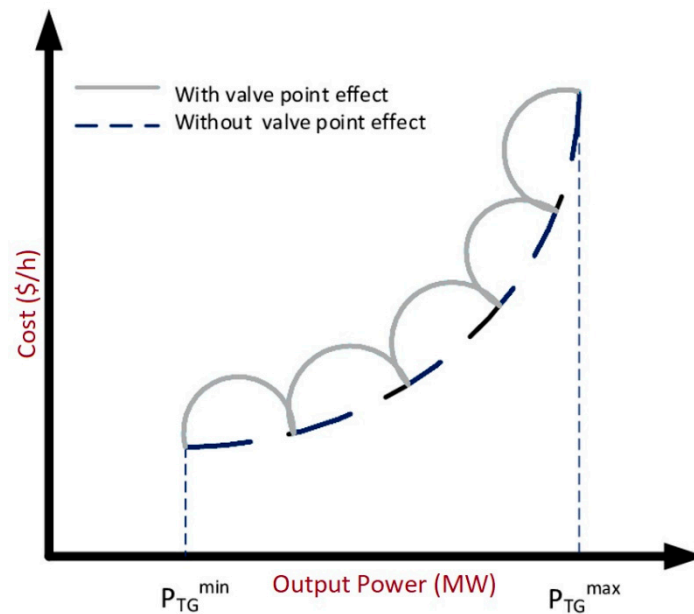


Figure 2. The output power with effects of valve point effect.

Table 2. Coefficients of thermal generators for cost and emission [24].

T_{G1}	T_{G2}	T_{G3}
Bus 1	Bus 2	Bus 8
$\Psi = -0.05554$ (t/p.u.MWh)	$\Psi = -0.06047$ (t/p.u.MWh)	$\Psi = -0.0355$ (t/p.u.MWh)
$\Phi = 0.04091$ (t/h)	$\Phi = 0.02543$ (t/h)	$\Phi = 0.05326$ (t/h)
$\zeta = 6.667$ (p.u.MW $^{-1}$)	$\zeta = 3.333$ (p.u.MW $^{-1}$)	$\zeta = 2$ (p.u.MW $^{-1}$)
$\tau = 0.0002$ (t/h)	$\tau = 0.0005$ (t/h)	$\tau = 0.002$ (t/h)
$\omega = 0.0649$ (t/p.u.MW 2 h)	$\omega = 0.05638$ (t/p.u.MW 2 h)	$\omega = 0.0338$ (t/p.u.MW 2 h)
$a = 30$ (\$/h)	$a = 25$ (\$/h)	$a = 20$ (\$/h)
$b = 2$ (\$/MWh)	$b = 1.75$ (\$/MWh)	$b = 3.25$ (\$/MWh)
$c = 0.00375$ (\$/MW 2 h)	$c = 0.0175$ (\$/MW 2 h)	$c = 0.00834$ (\$/MW 2 h)
$d = 18$ (\$/h)	$d = 16$ (\$/h)	$d = 12$ (\$/h)
$e = 0.037$ (rad/MW)	$e = 0.038$ (rad/MW)	$e = 0.045$ (rad/MW)

2.3. Price of Periodic and Stochastic Renewable Energy Plants

Integration of renewable plants into the power grid is difficult due to the periodic and stochastic characteristics of nature. Generally, PV farms, wind farms, etc. are inherited by non-public organizations which endure a buy consensus with the independent system operator (ISO) for a specific volume of scheduled power. The ISO is responsible for diminishing the shortage amount of the scheduled power if these renewable sources are insufficient or non-available. Thus, the spinning reserve must be kept if there is a demand. This situation is termed as an overestimation of renewable sources like windfarm and solar-farm and it adds extra cost for the ISO. Conversely, a condition may occur when

these renewable sources generate more power than the scheduled power which is called underestimation. In this case, the extra generated power can be wasted due to the non-utilization. So, the ISO must endure the penalty fee. Hence every cost for these renewable energy plants contains direct cost parallel to the scheduled power, an overestimation fee on account of the spinning reserve, and penalty prices owing to the underestimation.

The direct fee of the windfarm as an objective of the scheduled power can be shown as [24]:

$$(P_{ws}) = g_w P_{ws} \quad (3)$$

where g_w specifies the direct fee coefficient of the wind plant. P_{ws} designates the scheduled power of the same unit.

Likewise, for the solar power unit, the direct fee related to the solar unit is [24]:

$$(P_{ss}) = h_s P_{ss} \quad (4)$$

where h_s indicates the direct price coefficient of the solar PV unit and P_{ss} specifies the scheduled power of the same unit.

There is a third hybrid power plant considered in this case study which is owned by a single non-public operator that contains a small-hydro power unit and a solar PV plant. The direct price coefficients for these plants are non-identical. The output of the small-hydro power plant differs in line with the movement speed of the river [27]. Nevertheless, because the volume of the small-hydro power unit is trivial in comparison with the requested load of the network, this source generally operates at maximum.

Direct price linked with the hybrid unit calculated as [24]:

$$C_{sh}(P_{ssh}) = C_{sh}(P_{ssh,s} + P_{ssh,h}) = h_s P_{ssh,s} + m_h P_{ssh,h} \quad (5)$$

where P_{ssh} indicates the scheduled output power from the hybrid plant, $P_{ssh,s}$ is the influence of the solar unit, and $P_{ssh,h}$ is the influence of the small-hydro unit. The coefficient of direct price for the solar plant is h_s like the previous, and for the small-hydro unit, the coefficient is m_h .

2.3.1. Computing Price of Stochastic Wind Power

As discussed previously, owing to the stochastic essence of wind energy, the power output can be insufficient compared to the scheduled amount. If such a case occurs, ISO must have enough operating reserve to diminish the demand. The price of operating reserve for the wind plant can be computed as [18]:

$$C_{Rw}(P_{ws} - P_{wav}) = K_{Rw}(P_{ws} - P_{wav}) = K_{Rw} \int_0^{P_{ws}} (P_{ws} - p_w) f_w(p_w) dp_w \quad (6)$$

where the reserve price coefficient K_{Rw} is for the wind unit and the real power available from the same unit is P_{wav} . The probability density function (PDF) for the wind unit is represented by $f_w(p_w)$. This is due to the changes in wind speed which can be seen in Equation (34).

If underestimation happened in any case, the output power from the wind unit could be wasted due to the non-utilization. To utilize it, the output power of the normal generators must be reduced. A penalty price cost must be paid by the ISO if such a case arises. Charge of the penalty for the wind plant is formulated as [18]:

$$C_{Pw}(P_{wav} - P_{ws}) = K_{Pw}(P_{wav} - P_{ws}) = K_{Pw} \int_{P_{ws}}^{P_{wr}} (p_w - P_{ws}) f_w(p_w) dp_w \quad (7)$$

where the penalty fee coefficient K_{P_w} is for the wind unit and the calculated output power of the same unit is P_{wr} .

2.3.2. Computing Price of Stochastic Solar Power

The method for calculating the over and underestimation of solar power is similar to the windfarm. Although, in windfarm, a well-known Weibull PDF is drawn, for solar radiation, lognormal PDF is mostly used [16,28]. For ease of calculation, like the idea which is explained in [18,29], penalty and reserve fees are formulated accordingly. The reserve price of the PV unit for overestimation is formulated as [18]:

$$C_{R_s}(P_{ss} - P_{sav}) = K_{R_s}(P_{ss} - P_{sav}) = K_{R_s} * f_s(P_{sav} < P_{ss}) * [P_{ss} - E(P_{sav} < P_{ss})] \quad (8)$$

where K_{R_s} is the coefficient of the reserve fee related to the solar power unit and P_{sav} is the actual accessible power for the same unit. The possibility of a solar output deficit event is represented by $f_s(P_{sav} < P_{ss})$ and $E(P_{sav} < P_{ss})$ is the prediction of solar output power beneath P_{ss} .

For the opposite case of overestimating the solar unit cost, the penalty fee for underestimation is formulated as [18]:

$$C_{P_s}(P_{sav} - P_{ss}) = K_{P_s}(P_{sav} - P_{ss}) = K_{P_s} * f_s(P_{sav} > P_{ss}) * [E(P_{sav} > P_{ss}) - P_{ss}] \quad (9)$$

where K_{P_s} is the coefficient of the penalty fee for the solar unit. The likelihood of solar power surplus is represented by $f_s(P_{sav} > P_{ss})$ and the possibility of PV power exceeding P_{ss} is $E(P_{sav} > P_{ss})$.

2.3.3. Computing Price of Stochastic Hybrid Unit

Massive facilities of hydro power have enormous pools, making them suitable sources of spinning reserve. However, because the capacity of small-hydro is tiny in comparison to network production and consumption, the operating reserve size of it may not matter to the ISO. In actuality, penalty or reserve fees may not apply to the non-public agents of small-hydro plants at all. The 3rd production unit in our instance is a hybrid system. It consists of a solar PV plant mixed with a small hydro plant. The small hydro plant's output is determined by the flow rate of the river, which is notorious to follow the Gumbel distribution [30,31]. The PV power plant is now eligible for penalty and reserve costs, similar to the one described previously. We include penalty fees for underestimated and reserved fees for overestimated entire quantities of power output from the hybrid unit, for calculation purposes. This is because the small hydro contributes around 10–20% only.

Subsequent Equation (10), the overestimation reserve fee of the power from the hybrid unit is [24]:

$$C_{R_{sh}}(P_{ssh} - P_{shav}) = K_{R_{sh}}(P_{ssh} - P_{shav}) = K_{R_{sh}} * f_{sh}(P_{shav} < P_{ssh}) * [P_{ssh} - E(P_{shav} < P_{ssh})] \quad (10)$$

where the coefficient $K_{R_{sh}}$ is for the reserve price of the hybrid plant, and the real available output power of the same plant is shown as P_{shav} . The possibility of the power shortage event of this hybrid unit is $f_{sh}(P_{shav} < P_{ssh})$ and $E(P_{shav} < P_{ssh})$ is the prediction of hybrid unit output power lower than P_{ssh} .

Following Equation (11), the underestimation penalty fee of the hybrid power output is [24]:

$$C_{P_{sh}}(P_{shav} - P_{ssh}) = K_{P_{sh}}(P_{shav} - P_{ssh}) = K_{P_{sh}} * f_{sh}(P_{shav} > P_{ssh}) * [E(P_{shav} > P_{ssh}) - P_{ssh}] \quad (11)$$

where the coefficient of penalty fee concerning the hybrid unit is $K_{P_{sh}}$, the possibility of the hybrid unit power surplus is given by $f_{sh}(P_{shav} > P_{ssh})$. The prediction of hybrid unit output power exceeding P_{ssh} is $E(P_{shav} > P_{ssh})$.

2.3.4. Emission

Both the atmosphere and environment are filled with noxious gases that are released from fossil-fueled thermal generators. These gases are air pollutants and harmful. The quantity of noxious gas emissions, like NO_x as well as SO_x , etc., fluctuates with the amount of production power generated, coming from Equation (12). Emission (t/h) can be shown as [18]:

$$Emission, E_{Tot} = \sum_{i=1}^{N_{TG}} \left[(\varphi_i + \psi_i P_{TG_i} + \omega_i P_{TG_i}^2) \times 0.01 + \tau_i e^{(\zeta_i P_{TG_i})} \right] \quad (12)$$

where φ_i , ψ_i , ω_i , τ_i and ζ_i are coefficients of emission related to the i_{th} thermal plant. All of the mentioned coefficients can be seen in Table 2.

2.4. Objectives of Optimization

To calculate the total price of generation, the cost of the thermal generators, as well as the direct price of the renewable power along with their reserve and penalty price, must be summed. Hence, the total price of 3 thermal generators, 1 wind generator, 1 solar generator, and 1 hybrid generator which is a combination of a small-hydro and a PV can be specified as the summation of Equations (2)–(11) [24]:

$$\begin{aligned} C_{Tot} = & C_T(P_{TG}) + [C_w(P_{ws}) + C_{Rw}(P_{ws} - P_{wav}) + C_{Pw}(P_{wav} - P_{ws})] \\ & + [C_s(P_{ss}) + C_{Rs}(P_{ss} - P_{sav}) + C_{Ps}(P_{sav} - P_{ss})] \\ & + [C_{sh}(P_{ssh}) + C_{Rsh}(P_{ssh} - P_{shav}) + C_{Psh}(P_{shav} - P_{ssh})] \end{aligned} \quad (13)$$

The objective function of multi-objective optimization [24]:

$$\min F(x) = [C_{Tot}, E_{Tot}, Error] \quad (14)$$

where C_{Tot} is the total cost, E_{Tot} is the total emission, and *Error* is referred to the system restrictions. The process is to minimize cost and emission at the same time, finding a balance between economic efficiency and environmental sustainability while not violating any system restrictions. There exist many inequality and equality restrictions in the EED problem. Those restrictions will be explained in the coming sections in more detail.

2.5. Equality Limitations

For immediate power balancing, equality constraints require that the generated real and reactive power be equal to all of the network's corresponding demands and losses [18].

$$P_{Gi} - P_{Di} - V_i \sum_{j=1}^{NB} V_j [G_{ij} \cos(\delta_{ij}) + B_{ij} \sin(\delta_{ij})] = 0 \quad \forall i \in NB \quad (15)$$

$$Q_{Gi} - Q_{Di} - V_i \sum_{j=1}^{NB} V_j [G_{ij} \sin(\delta_{ij}) - B_{ij} \cos(\delta_{ij})] = 0 \quad \forall i \in NB \quad (16)$$

where $\delta_{ij} = \delta_i - \delta_j$, represents the distinction in voltage gradient of bus i as well as bus j . Real load demand related to the bus i is P_{Di} and reactive load demand for the same bus is Q_{Di} while for the same bus, P_{Gi} and Q_{Gi} are real and reactive power generation, respectively, from a conventional or renewable source. NB indicates overall buses in the system. The conductance being G_{ij} between bus i and j , and the susceptance being B_{ij} between bus i and j .

2.6. Inequality Limitations

In the EED problem, the inequality limitations consist of prohibited/forbidden operating zones (POZ) for thermal generators, operational limitation range of all generators in the system, and security limitations for buses as well as the transmission lines. In Equations (17)–(20) limitations for the actual power production of the thermal unit, wind plant, solar generator,

and hybrid unit are given, respectively, while Equations (21)–(24) specify the imaginary power limitations of the same generators with the same order.

Generator constraints for operational limitation range [24]:

$$P_{TGi}^{\min} \leq P_{TGi} \leq P_{TGi}^{\max} \quad \forall i \in N_{TG} \quad (17)$$

$$P_{ws}^{\min} \leq P_{ws} \leq P_{ws}^{\max} \quad (18)$$

$$P_{ss}^{\min} \leq P_{ss} \leq P_{ss}^{\max} \quad (19)$$

$$P_{ssh}^{\min} \leq P_{ssh} \leq P_{ssh}^{\max} \quad (20)$$

$$Q_{TGi}^{\min} \leq Q_{TGi} \leq Q_{TGi}^{\max} \quad \forall i \in N_{TG} \quad (21)$$

$$Q_{ws}^{\min} \leq Q_{ws} \leq Q_{ws}^{\max} \quad (22)$$

$$Q_{ss}^{\min} \leq Q_{ss} \leq Q_{ss}^{\max} \quad (23)$$

$$Q_{ssh}^{\min} \leq Q_{ssh} \leq Q_{ssh}^{\max} \quad (24)$$

Prohibited operating zones (POZ) are introduced to avoid discontinuity of the cost curve of thermal generators. Sometimes thermal generators cannot operate in the whole range and this happens because of different reasons like shaft bare quivering, a flaw in the generator itself, or its attachments like boilers, pumps, etc [32]. POZs can be represented as [24]:

$$P_{TGi}^{\min\text{poz},j} < \text{POZ}_{TGi}^j < P_{TGi}^{\max\text{poz},j} \quad (25)$$

where the lower bound and upper bound of the j^{th} POZ are $P_{TGi}^{\min\text{poz},j}$ and $P_{TGi}^{\max\text{poz},j}$, respectively, for the i^{th} thermal unit.

System security constraints can be shown as [24]:

$$V_{Gi}^{\min} \leq V_{Gi} \leq V_{Gi}^{\max} \quad \forall i \in NG \quad (26)$$

$$V_{Lp}^{\min} \leq V_{Lp} \leq V_{Lp}^{\max} \quad \forall p \in NL \quad (27)$$

$$S_{lq} \leq S_{lq}^{\max} \quad \forall q \in nl \quad (28)$$

Limitations of the voltage for the generator buses are shown in Equation (26) and NG is the number of generators whether it is renewable or generator bus. Voltage limitations for the load buses are represented in Equation (27) while limitations of the line are specified in Equation (28). NL is the number of load buses in the system while nl is the value of transmission lines inside the system.

Out of the abovementioned different limitations, equality boundaries of balancing power are satisfied by default, when the convergence of power flow happens. MATPOWER [33] is used with applying the Newton-Raphson method for performing and calculating the power flow.

Generator bus voltages and generator real power (excluding slack bus) are automatically handled for their inequality constraints. Within their specified range, the optimization algorithm selects a feasible solution that contains sets of control variables. If a generator is within the POZs, the algorithm must not select that value for decision variables. In other words, the algorithm is only allowed to select the values which are not in the range of POZs. An appropriate handling technique for remaining inequality boundaries is a must so that their limitations are all held correctly.

Some parameters like power loss of the system shown in Equation (29) and voltage deviation (VD) shown in Equation (30), which shows that the quality of voltage in the

system is considered. VD can be calculated by summing voltage deviations for all load buses in the system [34].

$$P_{loss} = \sum_{q=1}^{nl} G_{q(ij)} \left[V_i^2 + V_j^2 - 2V_i V_j \cos(\delta_{ij}) \right] \quad (29)$$

where, $\delta_{ij} = \delta_i - \delta_j$, represents the voltage angle difference of buses i and j and $G_{q(ij)}$ is the transfer conductance related to branch q which connects bus i and bus j .

$$VD = \sum_{p=1}^{NL} |V_{Lp} - 1| \quad (30)$$

2.7. Computing Uncertain Production of Renewable Power Sources

2.7.1. Distribution Probability of Power for Renewable Sources

For representing wind speed, Weibull PDF is mainly used [18]. The speed of the wind (v) m/s possibility is formulated as [18]:

$$f_v(v) = \left(\frac{\beta}{\alpha} \right) \left(\frac{v}{\alpha} \right)^{(\beta-1)} e^{-(v/\alpha)^\beta} \quad for \quad 0 < v < \infty \quad (31)$$

where α is the scale parameter and β is the shape of Weibull characteristics, respectively. Values for all PDF parameters can be seen in Table 3. These values are selected rationally with consideration of the capacity installed for power generation sources and most of them are the same as in Ref. [18]. In buses 5 and 11, a Monte-Carlo simulation of 8000 sample size was obtained from ref [24] for wind speed and solar irradiance distribution, respectively. The same goes for bus 13 which has a solar and small hydro plant. Hence, Weibull, Lognormal, and Gumbel fitting were applied according to the values of Table 3.

Table 3. All parameters of PDF for probability modeling of renewable energy [24].

Bus 5	Bus 11	Bus 13	Bus 13
Wind Plant	Solar Plant	Solar Plant	Hydro Plant
$\alpha = 9, \beta = 2$	$\mu = 5.2, \sigma = 0.6$	$\mu = 5.2, \sigma = 0.6$	$\lambda = 15, \gamma = 1.2$
75 MW	50 MW	45 MW	5 MW

For solar insolation distribution (G_s), lognormal PDF is used and it can specify the possibility of it as [18]:

$$f_G(G_s) = \frac{1}{G_s \sigma \sqrt{2\pi}} \exp \left\{ -\frac{(\ln G_s - \mu)^2}{2\sigma^2} \right\} \quad for \quad G_s > 0 \quad (32)$$

where μ is the mean and σ is the standard deviation of the lognormal PDF.

Distribution of Gumbel can represent the flow rate of the river as [24]:

$$f_Q(Q_h) = \frac{1}{\gamma} \exp \left(\frac{Q_h - \lambda}{\gamma} \right) \exp \left[-\exp \left(\frac{Q_h - \lambda}{\gamma} \right) \right] \quad (33)$$

where λ is the location parameter, γ is the scale, and Q_h is the flow rate of the river.

2.7.2. Production Power of PV, Small-Hydro and Wind Plants

At bus 5 there are 25 turbines and each of them has a 3 MW capacity, making the capacity of the wind farm 75 MW in total. The output power of the turbines is non-identical

due to the different wind speeds they face. The output power of the wind plant associated with wind speed can be designated as [18]:

$$p_w(v) = \begin{cases} 0, & \text{for } v < v_{in} \text{ and } v > v_{out} \\ p_{wr} \left(\frac{v-v_{in}}{v_r-v_{in}} \right) & \text{for } v_{in} \leq v \leq v_r \\ p_{wr} & \text{for } v_r < v \leq v_{out} \end{cases} \quad (34)$$

where the evaluated output of a wind plant is p_{wr} . Cut-in speed, cut-off speed, and rated speed of a wind plant are v_{in} , v_r and v_{out} , respectively. Enercon E82-E4 wind turbine has been considered in this case study which has a v_{in} of 3m/s, v_r of 16m/s, and v_{out} of 25m/s.

Energy transformation of the PV concerning solar insolation is [18]:

$$P_s(G_s) = \begin{cases} P_{sr} \left(\frac{G_s^2}{G_{std}R_c} \right) & \text{for } 0 < G_s < R_c \\ P_{sr} \left(\frac{G_s}{G_{std}} \right) & \text{for } G_s \geq R_c \end{cases} \quad (35)$$

where in a normal environment, G_{std} is the solar insolation and set to 1000 W/m². The specific insolation point is shown by R_c and set to 120 W/m². The evaluated output power of the solar unit is shown by P_{sr} and all these values are true for both of the PVs connected to buses 11 and 13.

The output power of the small-hydro unit is mathematically calculated as [27]:

$$P_H(Q_h) = \eta \rho g Q_h H_{hyd} \quad (36)$$

where Q_h is the flow rate of the water, H_{hyd} is the productive pressure head, the effectiveness of turbine-generator joining is η , the water density is shown with ρ and gravity acceleration is g . These values are set as $H_{hyd} = 25$ m, $\eta = 0.85$, $\rho = 1000$ kg/m³ and $g = 9.81$ m/s².

2.7.3. Computation of Probabilities of Wind Power

In zones beneath the cut-in speed or beyond the cut-off speed, the output production of the wind turbine is zero. When the wind speed is in the zone between rated and cut-off speed, the output power of the turbine is p_{wr} . The possibility of wind power output for these separate zones can be calculated as [35]:

$$f_w(p_w)\{p_w = 0\} = 1 - \exp\left[-\left(\frac{v_{in}}{\alpha}\right)^\beta\right] + \exp\left[-\left(\frac{v_{out}}{\alpha}\right)^\beta\right] \quad (37)$$

$$f_w(p_w)\{p_w = p_{wr}\} = \exp\left[-\left(\frac{v_r}{\alpha}\right)^\beta\right] - \exp\left[-\left(\frac{v_{out}}{\alpha}\right)^\beta\right] \quad (38)$$

where wind speed is shown with v , cut-in speed is v_{in} , cut-off speed is v_{out} , and evaluated/rated wind speed is v_r .

When the speed of the wind is in the zone between cut-in and rated speed, wind output power probability which is continuous can be formulated as [18]:

$$f_w(p_w) = \frac{\beta(v_r - v_{in})}{\alpha^\beta * p_{wr}} \left[v_{in} + \frac{p_w}{p_{wr}}(v_r - v_{in}) \right]^{\beta-1} \exp\left[-\left(\frac{v_{in} + \frac{p_w}{p_{wr}}(v_r - v_{in})}{\alpha}\right)^\beta\right] \quad (39)$$

2.7.4. Computing over and Underestimation Price of Production for PV Unit

Acquiring all of the available power of a PV plant may not be possible due to the limited capacity of the plant and its accessories. Furthermore, the non-public owner of the PV unit may not be eligible to pay the penalty fee above the evaluated capacity of the unit. The actual power of the PV unit that can be carried out can be represented by a scheduled

power. Scheduled power is the quantity that is commonly accepted between the non-public operator and ISO. The overestimation price in Equation (8) can be achieved with [18]:

$$C_{R_s}(P_{ss} - P_{sav}) = K_{R_s}(P_{ss} - P_{sav}) = K_{R_s} \sum_{n=1}^{N_b^-} [P_{ss} - P_{sn-}] * f_{sn-} \quad (40)$$

where the accessible power is shown with P_{sn-} and P_{ss} is the scheduled power. f_{sn-} is the comparative frequency of P_{sn-} and the number of PDF duos (P_{sn-} , f_{sn-}) generated is specified with N_b^- . According to Ref [24], a bigger number of portions (bins) does not significantly make the outcome better. Hence, to be practical, an overall number of 30 bins are chosen for N_b .

ISO must endure a defined penalty price of underestimation for the power of the solar plant. The penalty price stated in Equation (9) is formulated as [18]:

$$C_{P_s}(P_{sav} - P_{ss}) = K_{P_s}(P_{sav} - P_{ss}) = K_{P_s} \sum_{n=1}^{N_b^+} [P_{sn+} - P_{ss}] * f_{sn+} \quad (41)$$

where the accessible power is shown with P_{sn+} . f_{sn+} is the comparative frequency of P_{sn+} and the number of PDF duos (P_{sn+} , f_{sn+}) generated is specified with N_b^+ .

2.7.5. Computing over and Underestimation Price of Production for Hybrid Unit

Calculation of this price was obtained from the same case study in Ref [24]. The chosen hydro plants connected to bus number 13, have greater evaluated power compared to available hydro-power computed from the stochastic flow rate of the river. Output power from the two plants is summed and then combined. As previously stated, the small-hydro plant may not be eligible for the penalty or reserve cost. Nevertheless, since the contribution of this unit is trivial compared to the total power, the penalty and reserve price are computed by counting the hydroplant out for ease.

Similar to Equation (40), the overestimation price for the combined network can be shown with [24]:

$$C_{R_{sh}}(P_{ssh} - P_{shav}) = K_{R_{sh}}(P_{ssh} - P_{shav}) = K_{R_{sh}} \sum_{n=1}^{N_b^-} [P_{ssh} - P_{shn-}] * f_{shn-} \quad (42)$$

where the accessible power is shown with P_{shn-} and P_{ssh} is the scheduled power. f_{shn-} is the comparative frequency of P_{shn-} and the number of PDF duos (P_{shn-} , f_{shn-}) generated is specified with N_b^- . Succeeding Equation (41), the underestimation price cost of the mixed system can be formulated as [24]:

$$C_{P_{sh}}(P_{shav} - P_{ssh}) = K_{P_{sh}}(P_{shav} - P_{ssh}) = K_{P_{sh}} \sum_{n=1}^{N_b^+} [P_{shn+} - P_{ssh}] * f_{shn+} \quad (43)$$

where the accessible power is shown with P_{shn+} and P_{ssh} is the scheduled power. f_{shn+} is the comparative frequency of P_{shn+} and the number of PDF duos (P_{shn+} , f_{shn+}) generated is specified with N_b^+ .

Table 4 [24] shows the evaluated direct, reserve, and penalty price coefficients of uncertain solar, small hydro, and wind power, respectively. As it can be seen, it is decided that the highest direct price coefficient belongs to wind energy and then solar energy and after that, hydro power. The reserve price coefficient is more than the corresponding direct price coefficient to maintain the spinning reserve, but the penalty price is less than the direct price for not using the accessible power.

Table 4. Fee (\$/MW) coefficients for the uncertain source of renewable plants.

Bus 5	Bus 11	Bus 13
Wind	Solar	Solar and Hydro
$g_w = 1.7$	$h_w = 1.6$	$m_w = 1.5$
$K_{Rw} = 3$	$K_{Rs} = 3$	$K_{Rsh} = 3$
$K_{Pw} = 1.4$	$K_{Ps} = 1.4$	$K_{Psh} = 1.4$

2.8. Multi-Objective Optimization

2.8.1. Constraint Handling Technique (CH)

The first introduction of CH to deal with infeasible solutions is presented in [36]. Later on, Deb [37] introduced a tolerance parameter to handle constraints by first converting equality constraints into inequality constraints. Modifying the tournament selection of the solution is one way to deal with constraints, where initially two random solutions are chosen from the population and the first-rated solution is selected from that two. Hence, there can be three different cases at maximum: In case (1), both solutions are viable. In case (2), one solution is viable and the other one is not, and in case (3) both are infeasible solutions. However, in this study, a slightly different method is used and named ‘constrained domination’ [38]. The ‘constrained domination’ definition for two solutions x_i and x_j happens when x_i dominate x_j with any of the subsequent rules to be true:

1. The solution x_i is viable whereas x_j is not feasible.
2. Both solutions x_i and x_j are infeasible except x_i has lesser overall boundaries violation and it can be calculated by normalizing all constraint violations and summing them together [38]:

$$CV(x) = \sum_{j=1}^J \langle \bar{g}_j(x) \rangle + \sum_{k=1}^K abs(\bar{h}_k(x)) \quad (44)$$

where the expected value $\langle \alpha \rangle$ is $-\alpha$, if $\alpha < 0$, otherwise it is zero. $\bar{g}_j(x)$ is the inequality constraint and $\bar{h}_k(x)$ is the equality constraint. The normalization process can be achieved by:

$$\bar{g}_j(x) = (\langle g_j(x) \rangle - \langle g_j \rangle_{\min}) / (\langle g_j \rangle_{\max} - \langle g_j \rangle_{\min}) \quad (45)$$

where $\langle g_j \rangle_{\min}$ and $\langle g_j \rangle_{\max}$ are minimum and maximum population constraint violations, respectively.

3. Both solutions x_i and x_j are viable and the first solution is superior to the latter by the following rules to be both true:
 - The solution x_i is not inferior to the solution x_j in any aspect.
 - The solution x_i is surely superior to the solution x_j in at least one aspect.

2.8.2. Crossover

Crossover is one of the genetic operators that support the blend of the genetic component of two or higher solutions [39]. It can be said that applying crossover is one of the major differentiating characteristics of a genetic algorithm [40]. Some examples of crossover methods for mixing the parent solution and producing offspring (child) are [41]:

1. partially-mapped crossover (PMX)
2. cycle crossover (CX)
3. order crossover operator one (OX)
4. order crossover operator two (OX2)
5. position-based crossover operator (POS)

It is very important to select a suitable crossover method since a specific crossover technique works best for a specific problem, for instance, edge recombination operator (ERO) [42] which was proven to work best for the Traveling Salesman Problems, or, the

enhanced version of it in [43] which further improved the performance of the mentioned ERO. Thus, in this study, Simulated Binary Crossover (SBX) [44] is used due to the fact that any solution can be created in the initialization phase and during the convergence phase, the focus of the search can be increased. In the SBX, to produce offspring c_1 and c_2 from parents y_1 and y_2 , first an accidental value u is constructed in the range between 0 and 1. Secondly, by using a polynomial probability distribution [44], the parameter β_q would be computed as [45]:

$$\beta_q = \begin{cases} (u\alpha)^{\frac{1}{\eta_c+1}} & \text{if } u \leq \frac{1}{\alpha} \\ \left(\frac{1}{2-u\alpha}\right)^{\frac{1}{\eta_c+1}} & \text{otherwise} \end{cases} \quad (46)$$

where $\alpha = 2 - \beta^{-(\eta_c+1)}$ and β is computed as [45]:

$$\beta = 1 + \frac{2}{y_2 - y_1} \min[(y_1 - y_l), (y_u - y_2)] \quad (47)$$

The range of the parameter y is $[y_l, y_u]$ and the distribution index of SBX is shown by η_c which can have any non-negative quantity. Changing η_c to a smaller quantity grants offspring to be created far away from parents while a larger quantity allows it to be created near the parents.

Offspring can be computed as [45]:

$$c_1 = 0.5[(y_1 + y_2) - \beta_q|y_2 - y_1|] \quad (48)$$

$$c_2 = 0.5[(y_1 + y_2) + \beta_q|y_2 - y_1|] \quad (49)$$

where $y_1 < y_2$ but modification can be made for $y_1 > y_2$.

2.8.3. Mutation

After the crossover, the next protagonist in GA is the mutation operator [39]. Since the mutation operator disturbs the solutions based on accidental changes, choosing the correct method is crucial. Constraints narrow the entire solution space into a feasible subspace. Hence, it is sometimes difficult to reach all points inside the solution space and because of that, a correct technique can lead to finding the optimum but an improper one can give bias advantage [39]. Not all mutation operators can ensure the action of finding the global optimum. In fact, some of them work best for one specific problem while for other problems they are not promising. Some known mutation operators are:

1. displacement mutation operator (DM)
2. exchange mutation operator (EM)
3. scramble mutation operator (SM)
4. inversion mutation operator (IVM)
5. insertion mutation operator (ISM)

In this study, a parameter-based mutation known as polynomial mutation [44] is used. Figure 3 shows a sample code of this operator. The procedure is as follows.

Every control variable has a probability pm to be disrupted. A random number t between 1 and the value of control variables (V) is calculated for every decision variable. If $t < pm$ then the following procedure is applied to mutate the variables.

```

real_mutation(value)
float value;
{
float delta, u;
if flip (p_mutation){
u = random(); /* a random number in (0,1) */
if (u<0.5)
delta = pow(2*u, (1.0/(n+1))) - 1.0;
else delta = 1.0 - pow(2*(1.0-u), (1.0/(n+1)));
}
else delta = 0.0; /* no mutation */
return (value + delta * Max_mut);
}

```

Figure 3. Pseudo code of mutation using the polynomial probability distribution.

First, a random number u is created in the range between 0 and 1, and the parameter δ_q is calculated as [45]:

$$\delta_q = \begin{cases} \left[2u + (1 - 2u)(1 - \delta)^{\eta_m + 1} \right]^{\frac{1}{\eta_m + 1}} - 1 & \text{if } u \leq 0.5 \\ 1 - \left[2(1 - u) + 2(u - 0.5)(1 - \delta)^{\eta_m + 1} \right]^{\frac{1}{\eta_m + 1}} & \text{otherwise} \end{cases} \quad (50)$$

where the distribution index of mutation is shown with η_m and can have any non-negative quantity. A larger quantity of η_m gives a stronger possibility of establishing offspring within the neighborhood of the parent and a tiny value allows a further solution to be established. For $y \in [y_l, y_u]$ the parameter δ is formulated as [45]:

$$\delta = \min[(y - y_l), (y_u - y)] / (y_u - y_l) \quad (51)$$

where y is the parent solution and the mutated offspring is computed as [45]:

$$c = y + \delta_q(y_u - y_l) \quad (52)$$

Mutation probability (pm) for this study is considered to be $1/V$ where V is the number of decision variables, 11 in this study.

2.8.4. Real Coded NSGA-II

In 1995, a non-dominated sorting genetic algorithm (NSGA) was presented by Srinivas and Deb [46] to solve problems of multi-objective optimization. The idea is based on a suggestion given by Goldberg in 1989 [47] and follows an even earlier application of GA introduced in 1984 by Schaffer [48] known as the VEGA algorithm, which opened new doors in the field of multi-objective optimization. Although this algorithm, VEGA, gave promising results at first, later on it encountered bias approaching some of the *pareto* optimal solutions. Like VEGA, NSGA had some of its problems over the years, such as the excessive computational difficulty of non-dominated sorting, the absence of elitism, and the necessity of defining a sharing parameter [49]. Deb, later on, enhanced his NSGA algorithm to address the above-mentioned issues, the one that is now called NSGA-II or Elitist Non-dominated Sorting Genetic Algorithm. In NSGA-II, there are three characteristics:

1. The elitist concept is used in the algorithm.
2. The algorithm uses a clear technique to preserve diversity.
3. Non-dominated solutions are highlighted in the algorithm.

Each concept will be summarized. Detailed descriptions and definitions are provided in [49].

2.8.5. Quick Non-Dominated Sorting Procedure

To determine if the answers of the first non-dominated front are dominated by one another, the simplest way is to compare all of the solutions with each other one by one. Completing this procedure for the first non-dominated front would result in the overall complexity of $O(MN^2)$ where O is the 'Bachmann–Landau' notation (big O notation), M is the number of objectives, and N is the population magnitude. Finding individuals in the second non-dominated level can be achieved by repeating the same procedure only without considering the answers of the first non-dominated front. Again, the same complexity of $O(MN^2)$ is needed and this fact is true for the third and fourth and all other non-dominated levels. Thus, a total complexity of $O(MN^3)$ is necessary for the worst-case scenario in which there exists only a single solution at each level, for N number of fronts.

Figure 4 shows a quicker method with the overall complexity of $O(MN^2)$. n_p means how many times the solution p is dominated, and S_p is a group of solutions dominated by p . It is worth mentioning that, even though the simplest approach has higher overall complexity, it only requires $O(MN)$ storage, whereas the quicker approach has less complexity but it requires $O(MN^2)$ storage.

```

for each  $p \in P$ 
   $S_p = \emptyset$ 
   $n_p = 0$ 
  for each  $q \in P$ 
    if  $(p \prec q)$  then
       $S_p = S_p \cup \{q\}$ 
    else if  $(q \prec p)$  then
       $n_p = n_p + 1$ 
  if  $n_p = 0$  then
     $p_{\text{rank}} = 1$ 
     $F_1 = F_1 \cup \{p\}$ 
 $i = 1$ 
while  $F_i \neq \emptyset$ 
   $Q_i = \emptyset$ 
  for each  $p \in F_i$ 
    for each  $q \in S_p$ 
       $n_q = n_q - 1$ 
    if  $n_q = 0$  then
       $q_{\text{rank}} = i + 1$ 
       $Q = Q \cup \{q\}$ 
   $i = i + 1$ 
 $F_i = Q$ 

```

Figure 4. Pseudo-code for a quicker approach of non-dominated sorting.

For the quicker approach, in the first non-dominated front, n_p for all of the solutions are set to zero. Next, for all those solutions with n_p as zero, every representative q of its set S_p is inspected, and its domination magnitude is shortened by one. Afterward, any member q reaching the domination count of zero is placed into another category Q and forms the second non-dominated front. Now, the above-mentioned technique is practiced to the members of Q to form the third non-dominated front and this operation goes on till every front is established. To compute the complexity of this method, in the first inner loop of Figure 5 (for each $p \in F_i$), since each entity can be part of a maximum of one front, the loop is performed N times exactly. As for the second inner loop (for each $q \in S_p$), each entity can dominate other members $N - 1$ time at most, and checking dominated individuals needs no more than M comparisons. Hence, the total complexity of $O(MN^2)$ [49].

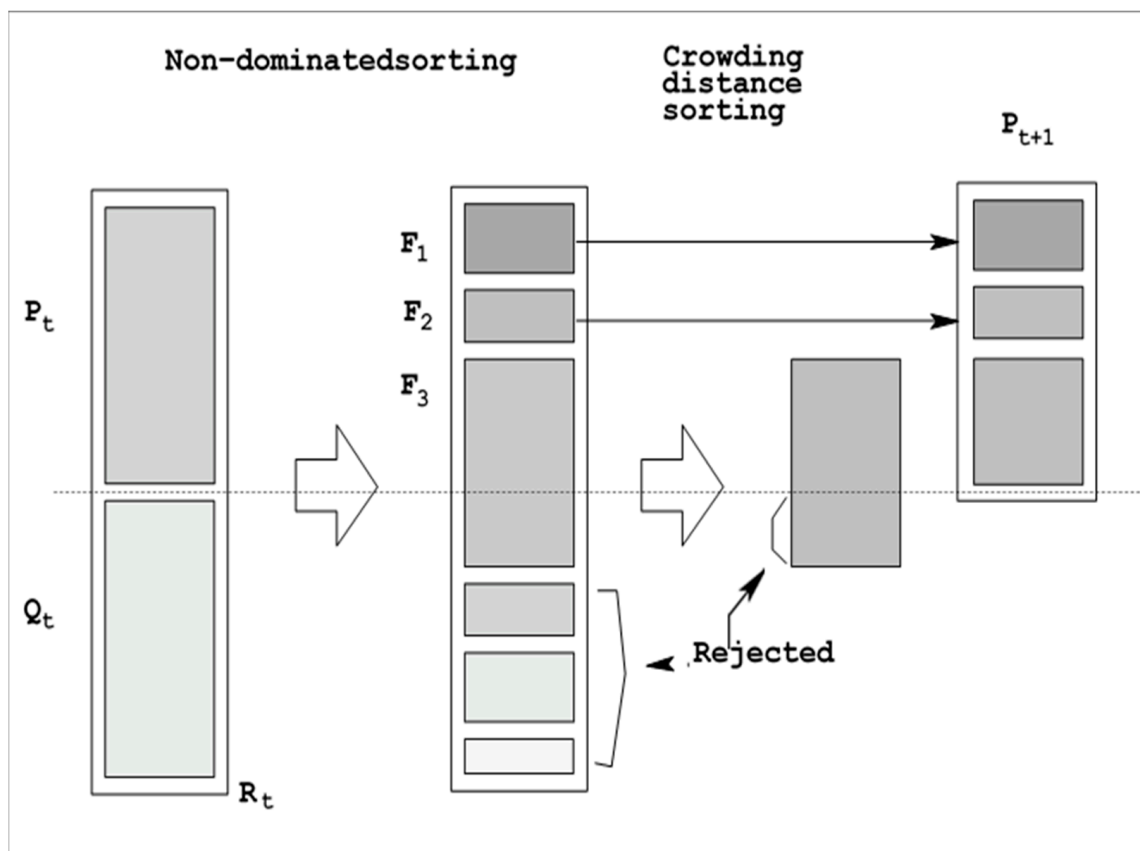


Figure 5. Illustration of the mechanism of NSGA-II.

2.8.6. Main Loop of NSGA-II

Firstly, an accidental parent population is generated which is called P_0 . Population sorting is built on non-domination. Every answer is given a rank corresponding to its non-domination position where rank 1 is the finest level, the best one afterward is rank 2, and the best one after that is rank 3, and it continues. Hence, minimizing the rank is expected. By using normal genetic operators like binary tournament selection, recombining, and mutating, the offspring Q_0 with a population of N is created. At this point, elitism is ready to be applied but first, a description of the t^{th} generation is necessary. The sample code of the t^{th} generation, by combining P_t and Q_t , a new population of size $2N$ is generated which is shown with R_t . Then, non-dominated sorting is enforced by blending the population with points of non-dominated fronts. Filling the population begins with selecting the points from the non-dominated front that has the highest rank (level 1 or F_1) and it continues with selecting the points of the non-dominated front with the second-best rank (level 2 or F_2) and so on. Because the capacity of R_t is limited to $2N$, there will be some fronts remaining.

The remaining fronts that cannot be accommodated, are removed. There also may be a situation when selecting points of the last front like F_3 in Figure 5, which are more than the needed slots for the new population. In this case, the points that add more diversity to the population are chosen. Here is one of the differences between NSGA-II and NSGA, where in the latter, a sharing parameter like δ is required for niching during the tournament selection and population reduction stage whereas in the former, a new method recognized as ‘crowding distance’ is represented. To calculate the diversity factor, a ‘crowding distance’ function is used. d_i is called the crowding distance of the point i and it is calculated by computing the objective space around the point i that is not inhabited by any other solution. d_i can be acquired by obtaining the cuboid’s perimeter shown in Figure 6. This cuboid is made with the assist of the closest neighbors of the point i . Now that the crowding distance is established, the points with the highest crowding distance value are selected for the new population until there is no slot left to fill and the remaining points are removed. Finally, a new population of P_{t+1} with the size of N is formed. In the next step, this population P_{t+1} is used to select, recombine and mutate for generating a new population Q_{t+1} with the size of N .

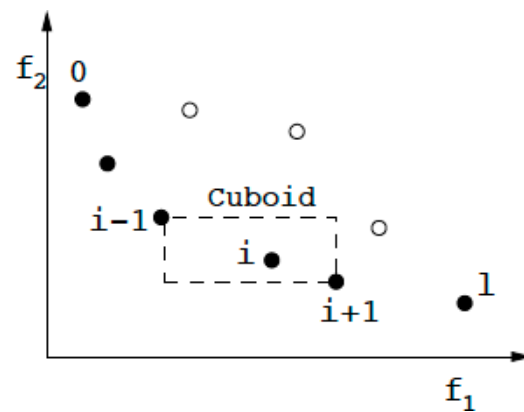


Figure 6. The crowding distance calculation.

The illustration in Figure 7 is showing how this new crowding distance function brings a new feature for selecting the fronts to be well diverse as the algorithm selects different solutions during the iteration.

```

 $R_t = P_t \cup Q_t$ 
 $F = \text{fast non-dominated sort } (R_t)$ 
 $P_{t+1} = \emptyset$  and  $i = 1$ 
until  $|P_{t+1}| + |F_i| \leq N$ 
    crowding distance assignment ( $F_i$ )
     $P_{t+1} = P_{t+1} \cup F_i$ 
     $i = i + 1$ 
Sort( $F_i$ , crowded comparison)
 $P_{t+1} = P_{t+1} \cup F_i [1 : (N - |P_{t+1}|)]$ 
 $Q_{t+1} = \text{make new population } (P_{t+1})$ 
 $t = t + 1$ 

```

Figure 7. Pseudo code of the t^{th} generation.

In Figure 8, the flowchart of how the algorithm works is represented. While having multiple objective functions along with constraints, the first step is to find trade-off solutions, meaning that one solution may not be absolutely better than the other one. In the second step, a single solution based on a method of choice like fuzzy decision-making [13,50], the same as in this study, will be extracted. An explanation of this method will be given at the end of this section.

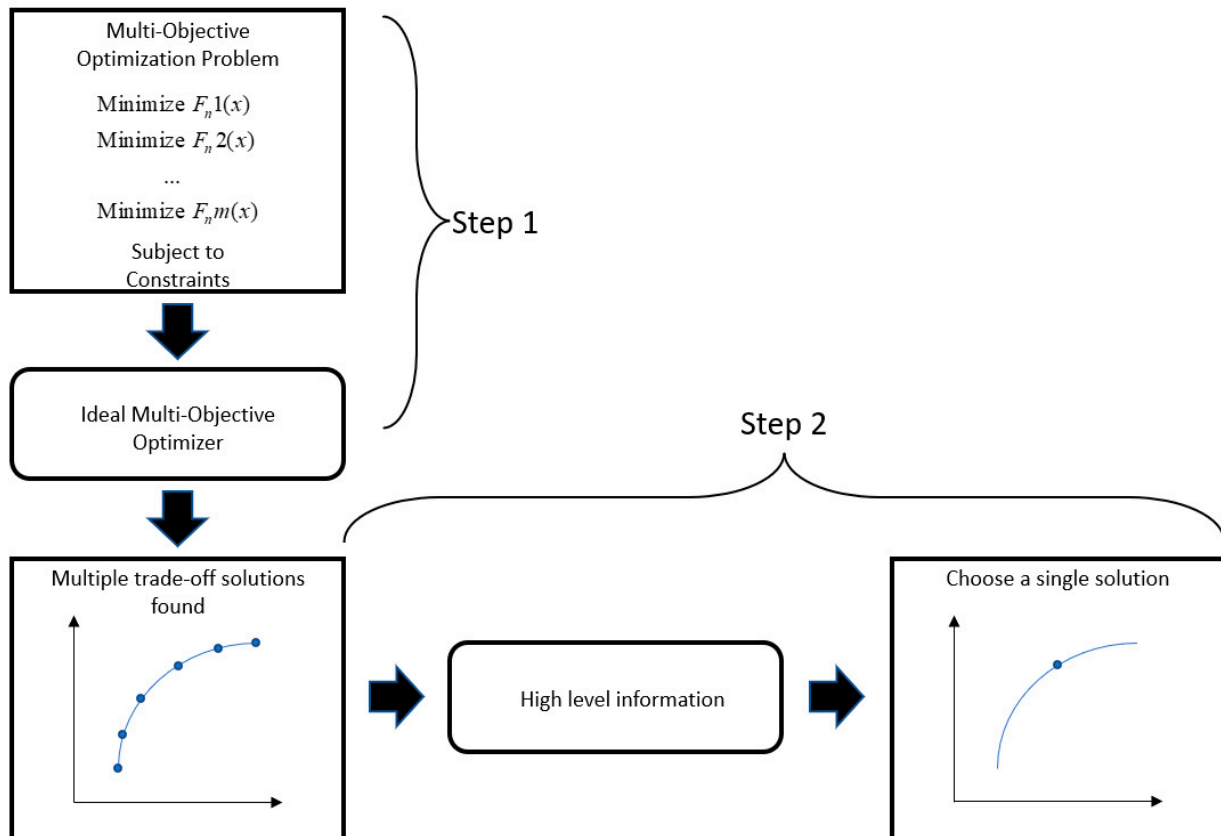


Figure 8. Illustration of a two-step multi-objective optimization mechanism.

2.9. Best Compromised Solution

2.9.1. Hypervolume Indicator

In a naive definition, a hypervolume indicator will consider the amount of area that is accumulated under or above a *pareto* front set while considering a set of reference points that is going to be needed for comparison. To make it simplified it can be said that the bigger the area is, the better the indicator becomes. Thus, the biggest output of the hypervolume indicator is the best [51,52]. A reference point is needed to measure the area under the curve. In this study, a set of reference points which are [1,1] has been chosen.

2.9.2. Steps of Calculating Compromised Solution

The method of calculating the best *pareto* front is a delicate formula. As mentioned before, there is no absolute best solution when comparing the results of multi-objective optimization. One algorithm can provide results for the best cost or emission on a single side of view, and it is easy to choose the best cost as an output target or the best emission for that matter, among all the available outcomes. However, when it comes to considering both cost and emission together, for instance, making cost better will result in making emission worse or vice versa. To overcome that, two steps can be taken while deciding on choosing the best result.

The first step is to choose the best result among all the results of the trial runs. To do that, a hypervolume indicator is used to determine which one of the *pareto* fronts is the best. Now, after this step, the best cost or the best emission can be chosen for comparison.

2.9.3. Fuzzy Decision Making

The second step is to designate the best-compromised solution out of the best *pareto* front. For that, fuzzy decision-making has been applied to obtain the best-compromised solution out of all answers in the best *pareto* front. The reason for that name is because while trying to make cost or emission better, the other objective would become worse in the process, hence compromise is needed. Comparing the compromised solution with each other may not make sense since no algorithm will give the best emission and the best cost at the same time. Thus, a technique must be used to extract the compromised results and, in this study, a fuzzy decision-making technique has been used. Computing fuzzy decision-making can be formulated as [24]:

$$\zeta_m^k = \begin{cases} 1 & \text{for } f_m^k \leq f_m^{\min} \\ \frac{f_m^{\min} - f_m^k}{f_m^{\max} - f_m^{\min}} & \text{for } f_m^{\min} < f_m^k < f_m^{\max} \\ 0 & \text{for } f_m^k \geq f_m^{\max} \end{cases} \quad (53)$$

where ζ_m^k defines the value of membership function for the m^{th} objective of the k^{th} non-dominated solution. M^{th} objective fitness value for the k^{th} non-dominated solution is shown with f_m^k , the maximum fitness number of the m^{th} objective function between all of the non-dominated answers is designated with f_m^{\max} and the minimum fitness value of the same function is represented with f_m^{\min} .

3. Results and Discussion

Throughout this section, the outcome of the simulation practicing real coded NSGA-II on the altered IEEE 30 bus case is examined and explained. The algorithm is described in Section 2. The initializing parameters are carefully selected and used for the method. They are listed below in Table 5.

Table 5. Defined parameters for real coded NSGA-II.

Parameter	Value
Size of the population	200
Maximum iteration amount	650
Distribution index of crossover, η_c	20
Distribution index for mutation, η_m	100
Number of decision variables, V	11
Number of runs	21
Mutation probability, pm	1/11

3.1. Simulation Results of the Algorithms

The size parameter defined in Table 5 is a standard population size, although, the maximum number of iterations is fine-tuned along with genetic operators of mutation and crossover. Mutation probability is also fine-tuned to give the best results. Table 6 will show the comparison of the hypervolume indicator. Decision variables are:

1. The actual power of the generator (excluding slack unit, P_{TG1})
2. Generator bus voltages from scheduled production of solar, wind, and hybrid (mixed solar and hydro) plants (P_{ws} , P_{ss} , and P_{ssh} , respectively)

Table 6. Comparison of HV numbers of algorithms.

Algorithm	Maximum	Minimum	Mean	Std Deviation
MOEA/D-SF	0.8352	0.8337	0.8346	0.0004
SMODE-SF	0.8707	0.8635	0.8684	0.0026
R-NSGA-II	0.8842	0.8577	0.8679	0.0071

POZs are introduced for thermal generator TG_2 to add discontinuity. The real power of P_{TG1} and the imaginary power of all generators are variables that are considered restrictions and should be satisfied by the algorithm. Accumulated voltage drops (VD) of load buses are also provided. The contribution of the small-hydro plant is shown with $P_{ssh,h}$.

We ran the simulations 21 times to observe the consistency and to be assured of the accuracy of the results. This way, we know that results did not happen by chance and we make sure they are consistent enough by measuring their standard deviations.

The hypervolume indicator has been calculated and compared. Table 6 shows a comparison between hypervolume indicator results from the algorithm in this study as well as two more algorithms from a previous study [24]. Min, max, and mean along with the standard deviation of the hypervolume indicator are displayed and compared, and R-NSGA-II has the highest hypervolume indicator with an acceptable standard deviation of less than 1 percent.

It is worth mentioning that the results across all 21 runs of the simulation are found to be consistent and it can be observed in Table 7 with a standard deviation of 0.0400. In Table 7 only the best cost of all 21 runs is provided. It can be seen that the lowest cost among the trial runs of the proposed algorithm is from run number 5, with a value of 892.7606 (\$/h) and the highest cost result calculated by the R-NSGA-II is from trial run number 11 with a value of 892.9335 (\$/h), which interestingly has the highest hypervolume indicator among all runs. This means that the results provided by the proposed R-NSGA-II in its worst-case scenario are better than the results provided by the other two algorithms in their best-case scenarios. Hence, the significance of the results and strength of the proposed approach are seen.

Table 7. Results of the cost of the R-NSGA-II optimization in all 21 runs of the simulation.

Run	Cost (\$/h)
1	892.7732
2	892.7820
3	892.7993
4	892.7728
5	892.7606
6	892.8236
7	892.7960
8	892.7701
9	892.7789
10	892.7790
11	892.9335
12	892.7886
13	892.7919
14	892.8735
15	892.7777
16	892.7877
17	892.7910
18	892.7631
19	892.7889
20	892.7670
21	892.7843

This is the starting point for showing the dominance of R-NSGA-II over the new techniques (MOEA/D-SF and SMODE-SF).

Comprehensive details of results along with settings of decision variables are presented in Table 8. The range of POZs is provided in Table 8. In Table 8, the best cost and the best emission are picked up from 21 runs of the simulation. In the first column, “Total fee” refers to C_{Tot} and “Emission” refers to E_{Tot} . Out of 21 runs, the one with the best (highest) hypervolume indicator was picked and is shown in the column “Comp”. In the fourth and fifth column, the best cost and the best emission is shown. They are the lowest value observed during all 21 runs. In the coming tables, the results of R-NSGA-II with two other algorithms will be compared in different scenarios to show the robustness of the developed algorithm.

Table 8. Simulation results of the R-NSGA-II optimization.

Control Variables	Min	Max	Cost	Emission	Comp
PTG1 (MW)	50	140	139.365	50.031	113.435
PTG2 (MW)					
POZ (for TG2): from [30,40] to [55,65]	20	80	54.066	48.861	65
PTG3 (MW)	10	35	11.206	34.455	20.525
P_{ws} (MW)	0	75	52.209	74.704	54.530
P_{ss} (MW)	0	50	17.639	49.198	18.964
P_{ssh} (MW)	0	50	15.445	28.572	16.444
$V_1(p.u.)$	0.95	1.10	1.0790	1.0671	1.0832
$V_2(p.u.)$	0.95	1.10	1.0645	1.0598	1.0691
$V_5(p.u.)$	0.95	1.10	1.0423	1.0454	1.0485
$V_8(p.u.)$	0.95	1.10	1.0397	1.0386	1.0367
$V_{11}(p.u.)$	0.95	1.10	1.0877	1.0729	1.0350
$V_{13}(p.u.)$	0.95	1.10	1.0608	1.0274	1.0386
$Q_{TG1}(MVar)$	−50	140	3.7384	10.021	13.474
$Q_{TG2}(MVar)$	−20	60	21.473	21.707	24.726
$Q_{TG3}(MVar)$	−15	40	39.771	33.554	38.055
$Q_{ws}(MVar)$	−30	35	26.316	25.922	31.426
$Q_{ss}(MVar)$	−20	25	24.997	24.436	9.3649
$Q_{ssh}(MVar)$	−20	25	20.570	10.359	15.708
Total fee (\$/h)			892.760	1017.4	924.864
Emission (t/h)			2.3231	0.0959	0.5111
VD (p.u.)			0.4524	0.4507	0.4753
$P_{ssh,h}$ (MW)			3.2648	3.0753	3.1518

The bolded area of Table 8, in the last column, shows the compromised solution that was extracted based on the highest hypervolume indicator as mentioned previously. This is highlighted to point out that the best-compromised result cannot be compared value by value to the other methods. Instead, the highest hypervolume indicator shows which algorithm has the best-compromised solution.

In Table 9, the results of two previously used methods along with the proposed method are provided. SMODE-SF, as well as MOEA/D-SF, are both performed in Ref. [24] with the same configuration.

Table 9. Comparison between R-NSGA-II and two previous algorithms in case of best pareto front (highest hypervolume indicator).

Control Variables	MOEA/D-SF		SMODE-SF		R-NSGA-II	
	Best Cost	Best Emission	Best Cost	Best Emission	Best Cost	Best Emission
PTG1 (MW)	139.297	62.280	139.112	50.072	139.731	50.005
PTG2 (MW)	55	70.051	55	52.627	55	52.228
PTG3 (MW)	10.622	35	10	34.919	10.490	34.823
P_{ws} (MW)	52.380	68.682	53.714	71.168	52.227	74.917
P_{ss} (MW)	17.348	31.034	16.167	29.555	17.614	49.686
P_{ssh} (MW)	15.328	19.509	16.057	48.254	14.965	24.513
$V_1(p.u.)$	1.0806	1.0690	1.0825	1.0732	1.0813	1.0805
$V_2(p.u.)$	1.0659	1.0653	1.0646	1.0572	1.0693	1.0689
$V_5(p.u.)$	1.0384	1.0473	1.0387	1.0076	1.0459	1.0448
$V_8(p.u.)$	1.0376	1.0420	1.0316	1.0302	1.0375	1.0370
$V_{11}(p.u.)$	1.0866	1.0681	1.0696	1.0691	1.0771	1.0046
$V_{13}(p.u.)$	1.0615	1.0582	1.0633	1.0160	1.0423	1.0271
$Q_{TG1}(MVar)$	5.317	−0.89	13.849	32.209	0.8551	24.718
$Q_{TG2}(MVar)$	26.047	27.845	21.72	29.609	33.465	29.655
$Q_{TG3}(MVar)$	37.51	34.543	32.692	36.783	37.359	34.835
$Q_{ws}(MVar)$	22.139	25.022	24.920	−5.19	28.204	21.447
$Q_{ss}(MVar)$	24.903	18.508	20.113	24.951	22.563	3.1901
$Q_{ssh}(MVar)$	21.131	20.416	23.70	8.624	14.565	13.571
Total fee (\$/h)	893.003	989.276	893.503	1018.786	892.933	1016.371
Emission (t/h)	2.3134	0.1091	2.2868	0.0961	2.3774	0.0961
$VD(p.u.)$	0.4464	0.4382	0.4304	0.5388	0.4305	0.5827
$P_{ssh,h}$ (MW)	3.50	3.20	3.131	3.254	3.2839	3.1603

Results of Table 9 are taken from the best *pareto* front of the best run among all 21 runs. Then, the ones with the lowest cost and emission are selected separately to be represented in the table as the best results of the cost and emission. It must be noted again, that these results are chosen according to the best hypervolume indicator of each optimization technique and they are not the absolute best cost/emission. It can be seen from the results that R-NSGA-II has the best cost among all the algorithms. As for the emission, it outperforms the MOEA/D-SF and gives the same emission value as SMODE-SF. It is fair to say that in the overall comparison, R-NSGA-II is superior to the other two algorithms despite the fact that R-NSGA-II is older and is supposed to perform worse. Further in this section, a detailed explanation regarding the superiority of R-NSGA-II will be given.

Comparison of the compromised solution with other methods

Table 10 represents the comparison between the discussed algorithms, solely based on their single objective value which is picked from one of the 21 runs of the simulation and gives the absolute best value for the cost and emission. The best-compromised solution was first picked from the run having the highest hypervolume indicator value and then extracted via the fuzzy decision-making method.

3.2. Detailed Analysis

To understand more about the superiority of the R-NSGA-II compared to the other two above-mentioned algorithms, analysis and explanation are provided in the next paragraphs. Take note that Table 10 has the absolute best value in case of cost, emission, and compromised solution.

Table 10. Comparison between R-NSGA-II and two previous methods in the case of best objectives.

Control Variables	Min	Max	MOEA/D-SF			SMODE-SF			Real Coded NSGA-II		
			Best Comp	Best Cost	Best Emission	Best Comp	Best Cost	Best Emission	Best Comp	Best Cost	Best Emission
PTG1 (MW)	50	140	117.118	139.048	60.003	111.91	139.848	50.047	113.435	139.365	50.031
PTG2 (MW)	20	80	65	53.763	65	65	55	47.535	65	54.066	48.861
PTG3 (MW)	10	35	18.403	11.558	34.890	23.555	10	35	20.525	11.206	34.455
P_{ws} (MW)	0	75	55.447	52.616	74.290	54.058	53.391	74.282	54.530	52.209	74.704
P_{ss} (MW)	0	50	17.649	17.593	28.529	18.436	16.818	50	18.964	17.639	49.198
P_{ssh} (MW)	0	50	15.326	15.319	23.755	15.755	14.989	29.336	16.444	15.445	28.572
$V_1(p.u.)$	0.95	1.10	1.076	1.0785	1.0545	1.0761	1.0823	1.0738	1.0832	1.0790	1.0671
$V_2(p.u.)$	0.95	1.10	1.0648	1.0644	1.0465	1.0662	1.0672	1.0596	1.0691	1.0645	1.0598
$V_5(p.u.)$	0.95	1.10	1.0444	1.0436	1.0277	1.0362	1.0406	1.0393	1.0485	1.0423	1.0454
$V_8(p.u.)$	0.95	1.10	1.0402	1.0398	1.0232	1.0362	1.0345	1.0196	1.0367	1.0397	1.0386
$V_{11}(p.u.)$	0.95	1.10	1.0878	1.0876	1.0619	1.0778	1.0743	1.0576	1.0350	1.0877	1.0729
$V_{13}(p.u.)$	0.95	1.10	1.0602	1.0622	1.0457	1.0432	1.0668	1.0481	1.0386	1.0608	1.0274
$Q_{TG1}(MVar)$	−50	140	2.128	2.736	8.771	2.788	7.191	28.944	13.474	3.7384	10.021
$Q_{TG2}(MVar)$	−20	60	21.410	21.153	19.405	34.504	27.547	21.749	24.726	21.473	21.707
$Q_{TG3}(MVar)$	−15	40	37.727	39.396	31.835	36.169	33.207	9.100	38.055	39.771	33.554
Q_{ws} (MVar)	−30	35	27.102	27.549	22.165	20.376	24.238	25.342	31.426	26.316	25.922
Q_{ss} (MVar)	−20	25	24.911	24.836	22.017	23.410	20.801	21.241	9.3649	24.997	24.436
Q_{ssh} (MVar)	−20	25	20.328	21.071	21.514	15.620	24.052	20.950	15.708	20.570	10.359
Total fee (\$/h)			919.040	892.954	994.342	927.049	893.314	1020.490	924.864	892.760	1017.4
Emission (t/h)			0.6221	2.2772	0.1052	0.4721	2.3950	0.0959	0.5111	2.3231	0.0959
VD (p.u.)			0.4530	0.4567	0.4542	0.4215	0.4369	0.468	0.4753	0.4524	0.4507
$P_{ssh,h}$ (MW)			3.50	3.50	3.135	3.296	3.163	3.183	3.1518	3.2648	3.0753

3.2.1. Superiority of the Proposed Method

When choosing the parameters of an optimization method, it is crucial to select the parameters that are best suited for the problem subjectively. As discussed before, SBX and polynomial mutation are best suited for this problem, hence making this approach provide better results even though this algorithm is older.

Comparing the total annual fee of the network is one way of showing robustness since the central objective of economic dispatch is to bring down the price. For that purpose, in the case that the best *pareto* front (highest hypervolume indicator) is selected, from Table 9, R-NSGA-II can save \$613.2 in a year compared to MOEA/D-SF and it can save \$4993.2 yearly compared to SMODE-SF. In another case where only the best individual cost is selected (out of 21 runs), from Table 10, R-NSGA-II saves \$1699.44 compared to the MOEA/D-SF method in a year, and it can save \$4853.04 each year compared to the SMODE-SF technique. R-NSGA-II also outperforms MOEA/D-SF in a single objective comparison of emission in Table 10. In the same table, although it gives the same emission as SMODE-SF, it can save \$27,068.4 yearly. In the case of a compromised solution, the best results (highest hypervolume indicator) belong to R-NSGA-II according to Table 6. Thus, R-NSGA-II is superior to the other algorithms in any measured aspect.

Table 11 illustrates the worst *pareto* front (lowest hypervolume indicator) among all 21 runs. Comparing the results of Table 10 with the results of Table 9 (best *pareto* front

of MOEDA/D-SF and SMODE-SF in this case), it can be observed that the R-NSGA-II dominates the MOEA/D-SF algorithm in the *best cost* section, meaning that the value of total cost (\$/h) and emission (t/h) provided by R-NSGA-II are lower and also in the *best emission* section, the value of emission (t/h) provided by R-NSGA-II is lower as well. When comparing the worst *pareto* front of R-NSGA-II with the best *pareto* front of SMODE-SF also, in the *best cost* section, R-NSGA-II is superior and in the *best emission* section, R-NSGA-II is not far behind.

Table 11. Worst *pareto* front (lowest hypervolume indicator) of the R-NSGA-II.

Control Variables	Min	Max	Cost	Emission	Comp
PTG1 (MW)	50	140	139.201	50.008	114.154
PTG2 (MW)	20	80	54.236	65	65
PTG3 (MW)	10	35	11.254	34.881	20.911
P_{ws} (MW)	0	75	52.220	74.231	55.205
P_{ss} (MW)	0	50	17.575	29.350	17.935
P_{ssh} (MW)	0	50	15.441	32.629	15.580
$V_1(p.u.)$	0.95	1.10	1.0801	1.0657	1.0760
$V_2(p.u.)$	0.95	1.10	1.0651	1.0615	1.0659
$V_5(p.u.)$	0.95	1.10	1.0423	1.0476	1.0420
$V_8(p.u.)$	0.95	1.10	1.0394	1.0411	1.0393
$V_{11}(p.u.)$	0.95	1.10	1.0866	1.0834	1.0817
$V_{13}(p.u.)$	0.95	1.10	1.0551	1.0663	1.0624
$Q_{TG1}(MVar)$	−50	140	5.5975	1.5613	0.9469
$Q_{TG2}(MVar)$	−20	60	21.707	19.965	26.886
$Q_{TG3}(MVar)$	−15	40	39.755	30.905	36.273
$Q_{ws}(MVar)$	−30	35	26.188	25.549	24.388
$Q_{ss}(MVar)$	−20	25	24.990	23.353	22.870
$Q_{ssh}(MVar)$	−20	25	18.600	22.310	21.581
Total fee (\$/h)			892.767	1006.8	923.28
Emission (t/h)			2.2993	0.0983	0.5030
VD (p.u.)			0.4387	0.4784	0.4469
$P_{ssh,h}$ (MW)			3.3403	2.9464	2.9494

3.2.2. Configuration and Characteristics of the Algorithm

Figure 9 displays the range of solutions provided by the R-NSGA-II and it is obtained from the best individual cases of cost and emission throughout the 21 runs. Figure 10 compares the best as well as the worst *pareto* front (highest and lowest hypervolume indicator) of the same method. The algorithm is well-diverse and the difference between the worst and best *pareto* fronts is trivial. In terms of convergence, the difference is negligible as well. The average time of calculation is 387.38 s for each trial. The R-NSGA-II is developed/coded using MATLAB and simulations are executed on a PC with an Intel Core i3 10th generation CPU @3.5 GHz and 8GB of RAM.

3.2.3. Critical Analysis

Voltage drop (VD) is an important factor to consider when designing electrical systems, as it can affect the performance of the circuit and the devices connected to it. Figure 11 displays all VD values for 21 runs of the simulation. It is desired to minimize voltage drop in order to maximize the efficiency and reliability of the system. Consistency of the VD values is shown in the same Figure 11 with 0.4165 as the minimum (the best) VD and 0.4607 being the maximum value (the worst) with a very good standard deviation of 0.0119 among all cases.

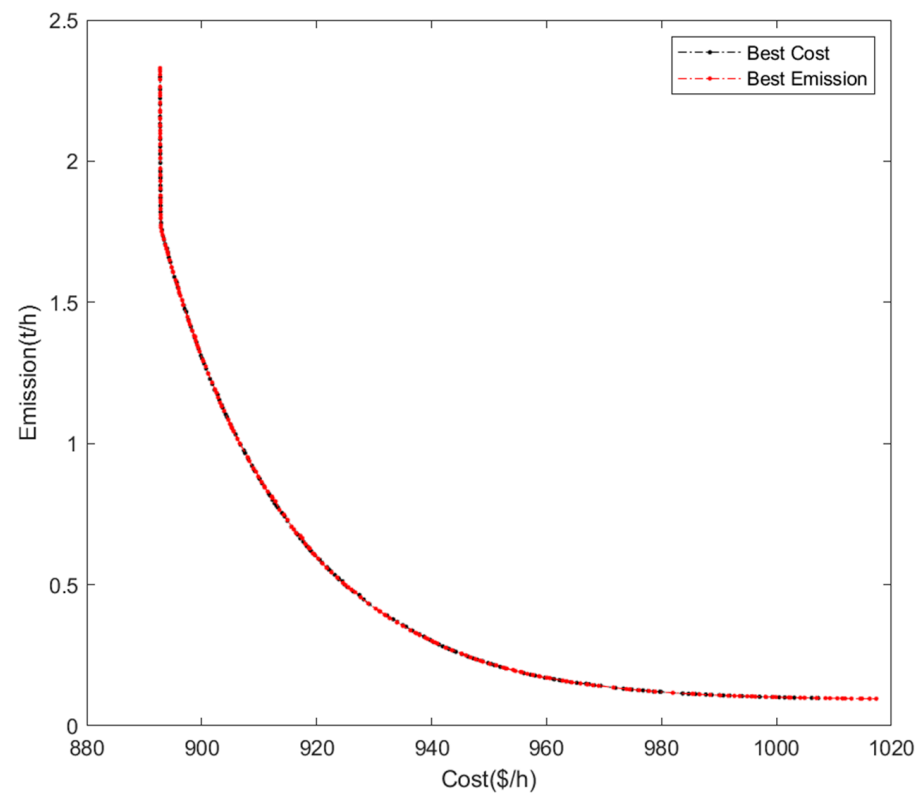


Figure 9. Pareto fronts of R-NSGA-II in the best and the worst cases.

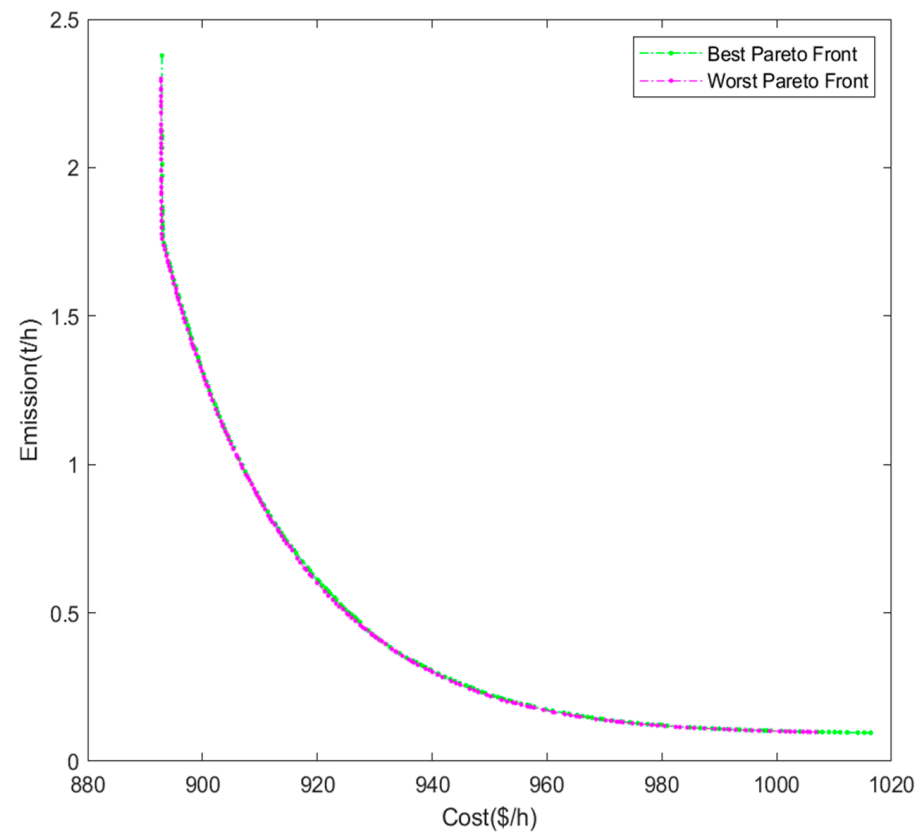


Figure 10. Best cost and emission of R-NSGA-II.

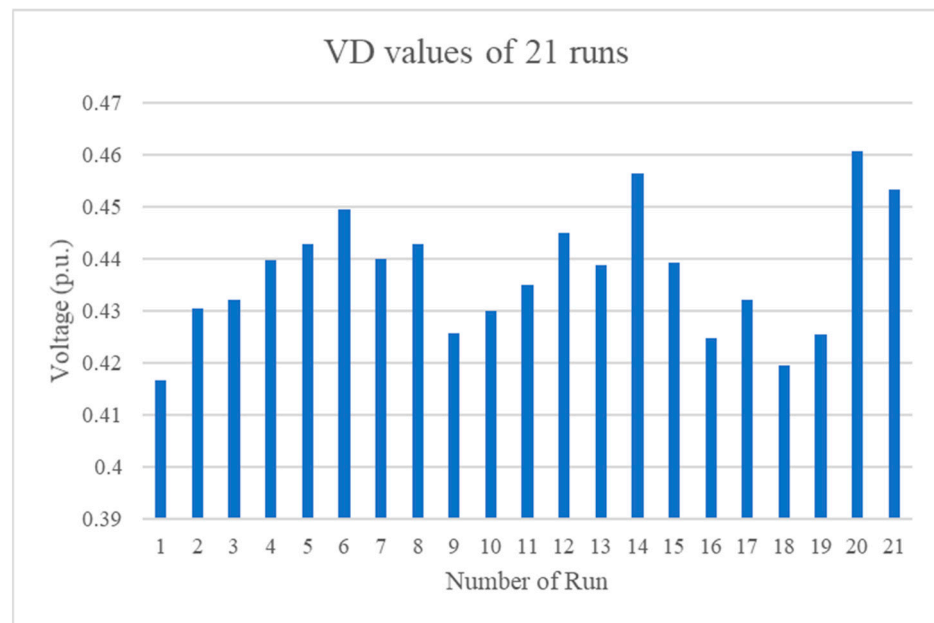


Figure 11. VD values for 21 runs of the simulation (R-NSGA-II).

In a previous study [24], the worst (highest) VD value provided by MOEA/D-SF among all 21 runs is reported to be 0.5704 p.u. and the same VD value for SMODE-SF is reported to be 0.6201 p.u. while the worst VD value provided by R-NSGA-II is 0.4607 p.u. and it means that R-NSGA-II not only can provide better cost and emission but also better reliability of the system. High voltage drop in an electrical system can cause a variety of problems:

- Reduced power quality: Electrical voltage fluctuations brought on by high voltage drops might result in reduced power quality.
- A rise in energy losses: As electricity travels through a conductor, heat is produced as a result of resistance. High voltage drops can result in significant energy losses, which lower system efficiency.
- Reduced system capacity: A system's capacity to transfer electrical power may be reduced if the voltage drop inside the system is too great. This may lower the system's ability to satisfy electricity demand.
- Increased operating costs: High voltage drops can result in greater energy losses and decreased system capacity, which can raise the system's running expenses.

It is crucial to keep an eye on voltage drops in electrical systems and take action to fix any issues that could be to blame.

Knowing that some of the generators are working near the limitation range of their reactive power, it is essential to have a practical constraint handling method like "constraint domination" which is used in this study. This will assure that while choosing the best solutions, critical points will not be thrown away with methods like the penalty factor. Figure 12 shows the reactive power schedule of generators for R-NSGA-II. It can be seen from the charts that some of the generators are working very close to their limits and do not have any violations. This is due to choosing a proper constraint handling method to ensure optimum performance while satisfying the system limitations.

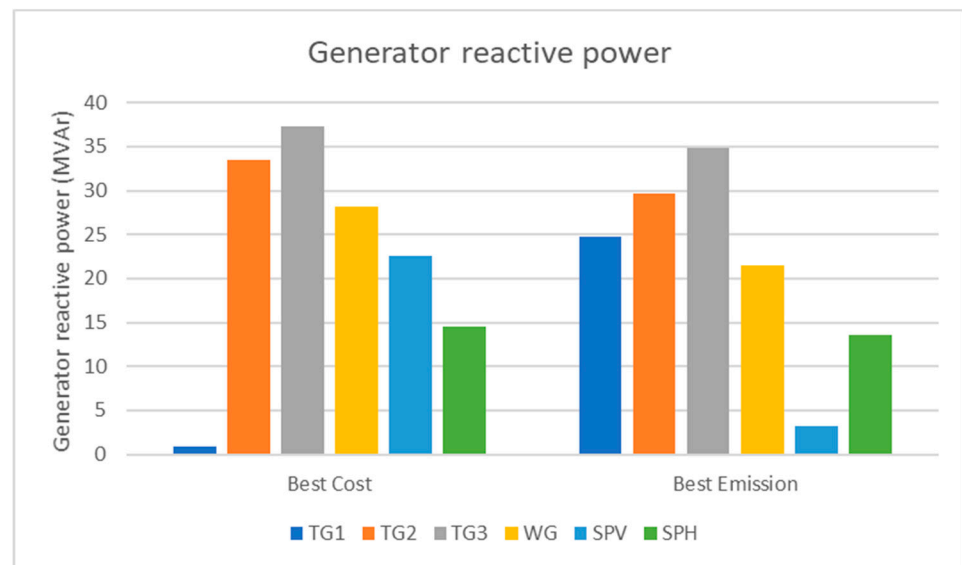


Figure 12. Generator reactive power usage (MVar) for R-NSGA-II.

We proved that R-NSGA-II is gaining better results but it is interesting to observe how different the operation of some generators is. R-NSGA-II has a value of 0.87 MVar for the TG1 generator in terms of best cost (Figure 12). Comparing the results of this study with the previous study [24], we can see that the TG1 generators in MOEA/D-SF and SMODE-SF methods are using approximately 5 to 17 times more power than R-NSGA-II, respectively, while other generators have the same mean value. It can be observed why R-NSGA-II is dominant, especially in terms of the best cost.

4. Conclusions

In this study, the MOEED (multi-objective economic and emission dispatch) which is a non-convex and non-linear problem was solved using the R-NSGA-II (real non-dominated sorting algorithm II), which was modified to include a better constraint handling method called “constraint domination”, and more suitable genetic operators: a mutation operator called “polynomial mutation”, and a crossover operator called simulated binary crossover (SBX). We used a standard IEEE 30-bus system and modified it to be incorporated with different renewable energy sources such as stochastic solar, small hydro, and wind units. With increasing concerns about clean energy and the policies of companies and governments, it is important to consider renewable energy sources in energy systems. To forecast the stochastic behavior of these sources, we used suitable probability density functions. We also embodied prohibited operating zones, valve point effect, and generator limitation in the design of a thermal unit. Network security was considered. MOEED was calculated by applying R-NSGA-II and results were compared to two previously studied algorithms: SMODE-SF and MOEA/D-SF. Even though R-NSGA-II is older than MOEA/D-SF and SMODE-SF, the results showed that R-NSGA-II outperforms the other two algorithms in terms of cost and emission, and this superiority was consistently observed in 21 runs of the algorithm and did not happen by chance. Not only that, R-NSGA-II also provided more security, stability, and quality of the system. This superiority was due to careful study of the subject matter, and selection of the genetic operators and constraint handling technique.

This study is beneficial in the energy sector since there is a limited number of articles that studied the process of optimizing MOEED in depth. Going emission-free is a serious issue and it is the goal of many countries and governments. The authors plan to continue studying MOEED in future works, possibly using newer approaches such as NSGA-III, etc. As smart grids become more prevalent, it is important to expand the literature on MOEED and its potential for emulating the behavior of energy systems, by using new technologies like digital twins.

Some limitations of this approach can be enhanced in future studies. These limitations/suggestions are: Taking into account life cycle cost analysis of renewable sources as part of the objective function since maintenance and disposal costs can impact the overall optimization process. It can be a good idea to consider electrical vehicles and battery systems for energy flexibility [53], this can be beneficial for MOEED and future smart grids. Decision-makers must also know the overall impact to see whether an investment in renewable units is beneficial/feasible or not, or how many renewables of different types must be considered to make the project feasible. A better policy for decision-making must be considered since policymakers need to pay attention to the lack of precise and certain data and the presence of conflicting goals when evaluating investments [22]. This again, can impact the overall process of calculation, optimization, and investment and consequently reduce emission and saving costs.

Author Contributions: M.L.A. was responsible for the conceptualization, methodology, software, validation, formal analysis, investigation, resources, data curation, writing—original draft preparation, writing—review and editing; R.S. was responsible for the conceptualization, methodology, validation, formal analysis, resources, data curation, writing—review and editing, supervision, project administration. All authors have read and agreed to the published version of the manuscript.

Funding: This research received no external funding.

Institutional Review Board Statement: Not applicable.

Informed Consent Statement: Not applicable.

Data Availability Statement: The data that support the findings of this study are available from the corresponding author upon reasonable request.

Conflicts of Interest: The authors declare no conflict of interest.

Nomenclatures

$f_G(G_s)$	Probability of solar irradiance G_s
$f_q(Q_w)$	Probability of river flow rate Q_w
$f_v(v)$	Probability of wind speed (v)
G_s	Solar irradiance
g_w	Direct fee coefficient related to the wind plant
h_s	Direct fee coefficient related to the solar unit
K_{Ps}	Penalty cost coefficient related to the solar plant underestimation
K_{Psh}	Penalty cost coefficient regarded with the hybrid plant
K_{Pw}	Penalty fee coefficient related to the wind plant underestimation power
K_{Rs}	Reserve cost coefficient related to the solar plant overestimation
K_{Rsh}	Reserve cost coefficient related to the hybrid plant
K_{Rw}	Reserve fee coefficient related to the wind plant overestimation power
m_h	Direct fee coefficient related to the hybrid unit
ms	Mutation probability
P_{hr}	Graded output power related to the small hydro plant
P_{loss}	Actual power loss in the system
P_{sav}	Actual accessible power related to the solar unit
P_{shav}	Actual accessible power related to the hybrid unit
P_{sr}	Graded output power of the solar unit
P_{ss}	Scheduled power related to the solar unit
P_{ssh}	Scheduled power related to the hybrid unit
P_{TGi}	Power output from the i^{th} thermal plant
P_{wav}	Actual accessible power related to the wind unit

p_{wr}	Graded output power of a wind plant
P_{ws}	Scheduled power related to the wind unit
Q_w	River flow rate
SF	Superiority of feasible answers
SPH	Combination of a solar and a small hydro plant
TG/T_G	Thermal power plant/generator
WG/W_G	Wind plant/generator
α, β	Weibull PDF's scale parameter and shape parameter respectively
λ, γ	Gumbel PDF's location specification and scale value respectively
μ, δ	Lognormal PDF's mean parameter and standard deviation respectively
CH	Constraint handling technique
ED	Economic dispatch
EED	Economic-environmental/emission dispatch
HV	Hypervolume indicator
ISO	Independent system agent/operator
$MOEA/D$	Decomposition-based method for multi-objective evolutionary algorithm
$MOEED$	Multi-objective economic emission dispatch
PDF	Probability density function
POZ	Prohibited/forbidden operating zone
PV	Photovoltaic
$R-NSGA-II$	Real coded non-dominated sorting genetic algorithm II
SBX	Simulated binary crossover
$SMODE$	Summation-based method for multi-objective differential evolution technique
VD	Voltage deviation aggregation of load buses in the system

References

- Planas, E.; Gil-De-Muro, A.; Andreu, J.; Kortabarria, I.; Martínez De Alegría, I. General aspects, hierarchical controls and droop methods in microgrids: A review. *Renew. Sustain. Energy Rev.* **2013**, *17*, 147–159. [\[CrossRef\]](#)
- Lasseter, R.H. Microgrids. In Proceedings of the 2002 IEEE Power Engineering Society Winter Meeting. (Cat. No. 02CH37309), New York, NY, USA, 27–31 January 2002; IEEE: Hoboken, NJ, USA, 2002; pp. 305–308.
- Júnior, J.D.A.B.; Nunes, M.V.A.; Nascimento, M.H.R.; Rodríguez, J.L.M.; Leite, J.C. Solution to economic emission load dispatch by simulated annealing: Case study. *Electr. Eng.* **2018**, *100*, 749–761. [\[CrossRef\]](#)
- Roy, P.K.; Bhui, S. A multi-objective hybrid evolutionary algorithm for dynamic economic emission load dispatch. *Int. Trans. Electr. Energy Syst.* **2016**, *26*, 49–78. [\[CrossRef\]](#)
- Júnior, J.D.A.B.; Nunes, M.V.A.; Nascimento, M.H.R.; Leite, J.C.; Rodríguez, J.L.M.; Freitas, C.A.O.D.; Júnior, M.F.; Oliveira, E.F.D.; Alencar, D.B.D.; Moraes, N.M.; et al. Multi-Objective Optimization Techniques to Solve the Economic Emission Load Dispatch Problem Using Various Heuristic and Metaheuristic Algorithms. *InTech Open* **2018**.
- Adarsh, B.R.; Raghunathan, T.; Jayabarathi, T.; Yang, X.-S. Economic dispatch using chaotic bat algorithm. *Energy* **2016**, *96*, 666–675. [\[CrossRef\]](#)
- Jayabarathi, T.; Raghunathan, T.; Adarsh, B.R.; Suganthan, P.N. Economic dispatch using hybrid grey wolf optimizer. *Energy* **2016**, *111*, 630–641. [\[CrossRef\]](#)
- Meng, A.; Li, J.; Yin, H. An efficient crisscross optimization solution to large-scale non-convex economic load dispatch with multiple fuel types and valve-point effects. *Energy* **2016**, *113*, 1147–1161. [\[CrossRef\]](#)
- Modiri-Delshad, M.; Aghay Kaboli, S.H.; Taslimi-Renani, E.; Rahim, N.A. Backtracking search algorithm for solving economic dispatch problems with valve-point effects and multiple fuel options. *Energy* **2016**, *116*, 637–649. [\[CrossRef\]](#)
- Di Somma, M.; Graditi, G.; Heydarian-Forushani, E.; Shafie-khah, M.; Siano, P. Stochastic optimal scheduling of distributed energy resources with renewables considering economic and environmental aspects. *Renew. Energy* **2018**, *116*, 272–287. [\[CrossRef\]](#)
- Secui, D.C. A new modified artificial bee colony algorithm for the economic dispatch problem. *Energy Convers. Manag.* **2015**, *89*, 43–62. [\[CrossRef\]](#)
- Ghasemi, A.; Gheydi, M.; Golkar, M.J.; Eslami, M. Modeling of Wind/Environment/Economic Dispatch in power system and solving via an online learning meta-heuristic method. *Appl. Soft Comput.* **2016**, *43*, 454–468. [\[CrossRef\]](#)
- Qu, B.Y.; Liang, J.J.; Zhu, Y.S.; Wang, Z.Y.; Suganthan, P.N. Economic emission dispatch problems with stochastic wind power using summation based multi-objective evolutionary algorithm. *Inf. Sci.* **2016**, *351*, 48–66. [\[CrossRef\]](#)
- Khan, N.A.; Awan, A.B.; Mahmood, A.; Razzaq, S.; Zafar, A.; Sidhu, G.A.S. Combined emission economic dispatch of power system including solar photo voltaic generation. *Energy Convers. Manag.* **2015**, *92*, 82–91. [\[CrossRef\]](#)
- Kheshti, M.; Kang, X.; Bie, Z.; Jiao, Z.; Wang, X. An effective Lightning Flash Algorithm solution to large scale non-convex economic dispatch with valve-point and multiple fuel options on generation units. *Energy* **2017**, *129*, 1–15. [\[CrossRef\]](#)
- Surender Reddy, S.; Bijwe, P.R.; Abhyankar, A.R. Real-Time Economic Dispatch Considering Renewable Power Generation Variability and Uncertainty Over Scheduling Period. *IEEE Syst. J.* **2015**, *9*, 1440–1451. [\[CrossRef\]](#)

17. Reddy, S.S. Optimal scheduling of thermal-wind-solar power system with storage. *Renew. Energy* **2017**, *101*, 1357–1368. [CrossRef]
18. Biswas, P.P.; Suganthan, P.N.; Amaratunga, G.A.J. Optimal power flow solutions incorporating stochastic wind and solar power. *Energy Convers. Manag.* **2017**, *148*, 1194–1207. [CrossRef]
19. Liu, G.; Zhou, J.; Xiao, X.; Li, M.; Yang, Y.; Lu, C. Dynamic Economic Dispatch in Thermal-Wind-Small Hydropower Generation System. *EDP Sci.* **2018**, *246*, ac415f. [CrossRef]
20. Salkuti, S.R. Multi-objective based economic environmental dispatch with stochastic solar-wind-thermal power system. *Int. J. Electr. Comput. Eng.* **2020**, *10*, 4543. [CrossRef]
21. Yalcinoz, T.; Rudion, K. Multi-objective Environmental-economic Load Dispatch Considering Generator Constraints and Wind Power Using Improved Multi-objective Particle Swarm Optimization. *Adv. Electr. Comput. Eng.* **2020**, *20*, 3–10. [CrossRef]
22. Hashemizadeh, A.; Ju, Y. Optimizing renewable energy portfolios with a human development approach by fuzzy interval goal programming. *Sustain. Cities Soc.* **2021**, *75*, 103396. [CrossRef]
23. Shafiekhani, M.; Hashemizadeh, A. 17-Multi-objective scheduling of a virtual power plant considering emissions. In *Scheduling and Operation of Virtual Power Plants*; Zangeneh, A., Moeini-Aghtaie, M., Eds.; Elsevier: Amsterdam, The Netherlands, 2022; pp. 377–397.
24. Biswas, P.P.; Suganthan, P.N.; Qu, B.Y.; Amaratunga, G.A.J. Multiobjective economic-environmental power dispatch with stochastic wind-solar-small hydro power. *Energy* **2018**, *150*, 1039–1057. [CrossRef]
25. Paish, O. Small hydro power: Technology and current status. *Renew. Sustain. Energy Rev.* **2002**, *6*, 537–556. [CrossRef]
26. Rawa, M.; Abusorrah, A.; Bassi, H.; Mekhilef, S.; Ali, Z.M.; Abdel Aleem, S.H.E.; Hasanien, H.M.; Omar, A.I. Economical-technical-environmental operation of power networks with wind-solar-hydropower generation using analytic hierarchy process and improved grey wolf algorithm. *Ain Shams Eng. J.* **2021**, *12*, 2717–2734. [CrossRef]
27. Wijesinghe, A.; Lai, L.L. Small Hydro Power Plant Analysis and Development. In Proceedings of the 2011 4th International Conference on Electric Utility Deregulation and Restructuring and Power Technologies (DRPT), Weihai, China, 6–9 July 2011; IEEE: Hoboken, NJ, USA, 2011; pp. 25–30.
28. Chang, T.P. Investigation on frequency distribution of global radiation using different probability density functions. *Int. J. Appl. Sci. Eng.* **2010**, *8*, 99–107.
29. Shi, L.; Wang, C.; Yao, L.; Ni, Y.; Bazargan, M. Optimal power flow solution incorporating wind power. *IEEE Syst. J.* **2011**, *6*, 233–241. [CrossRef]
30. Mujere, N. Flood frequency analysis using the Gumbel distribution. *Int. J. Comput. Sci. Eng.* **2011**, *3*, 2774–2778.
31. Cabus, P. River flow prediction through rainfall–runoff modelling with a probability-distributed model (PDM) in Flanders, Belgium. *Agric. Water Manag.* **2008**, *95*, 859–868. [CrossRef]
32. Jadhav, H.T.; Roy, R. Gbest guided artificial bee colony algorithm for environmental/economic dispatch considering wind power. *Expert Syst. Appl.* **2013**, *40*, 6385–6399. [CrossRef]
33. Zimmerman, R.D.; Murillo-Sánchez, C.E. Matpower 7.1. Available online: <https://matpower.org> (accessed on 12 September 2020).
34. Biswas, P.P.; Suganthan, P.N.; Mallipeddi, R.; Amaratunga, G.A. Optimal power flow solutions using differential evolution algorithm integrated with effective constraint handling techniques. *Eng. Appl. Artif. Intell.* **2018**, *68*, 81–100. [CrossRef]
35. Dubey, H.M.; Pandit, M.; Panigrahi, B. Hybrid flower pollination algorithm with time-varying fuzzy selection mechanism for wind integrated multi-objective dynamic economic dispatch. *Renew. Energy* **2015**, *83*, 188–202. [CrossRef]
36. Powell, D.; Skolnick, M.M. Using Genetic Algorithms in Engineering Design Optimization with Non-Linear Constraints. In Proceedings of the 5th International conference on Genetic Algorithms, San Francisco, CA, USA, 1 June 1993; IEEE: Hoboken, NJ, USA, 1993; pp. 424–431.
37. Deb, K. An efficient constraint handling method for genetic algorithms. *Comput. Methods Appl. Mech. Eng.* **2000**, *186*, 311–338. [CrossRef]
38. Deb, K. Multi-objective optimisation using evolutionary algorithms: An introduction. In *Multi-Objective Evolutionary Optimisation for Product Design and Manufacturing*; Springer: Berlin, Germany, 2011; pp. 3–34.
39. Kramer, O. Genetic algorithms. In *Genetic Algorithm Essentials*; Springer: Berlin, Germany, 2017; pp. 11–19.
40. Mitchell, M. *An Introduction to Genetic Algorithms*; MIT Press: London, UK, 1998.
41. Starkweather, T.; McDaniel, S.; Mathias, K.E.; Whitley, L.D.; Whitley, C. *A Comparison of Genetic Sequencing Operators*; ICGA: Southport, Australia, 1991; pp. 69–76.
42. Whitley, D.; Starkweather, T. Genitor II: A distributed genetic algorithm. *Journal of Experimental & Theoretical Artificial Intelligence* **1990**, *2*, 189–214.
43. Whitley, D.; Starkweather, T.; Shaner, D. *The Traveling Salesman and Sequence Scheduling: Quality Solutions Using Genetic Edge Recombination*; Citeseer: New York, NY, USA, 1991.
44. Deb, K.; Agrawal, R.B. Simulated binary crossover for continuous search space. *Complex Syst.* **1995**, *9*, 115–148.
45. Deb, K.; Agrawal, S. A Niche-Penalty Approach for Constraint Handling in Genetic Algorithms. In *Artificial Neural Nets and Genetic Algorithms*; Springer: Berlin, Germany, 1999; pp. 235–243.
46. Srinivas, N.; Deb, K. Multiobjective optimization using nondominated sorting in genetic algorithms. *Evol. Comput.* **1994**, *2*, 221–248. [CrossRef]
47. Goldberg, D.E.; Korb, B.; Deb, K. Messy genetic algorithms: Motivation, analysis, and first results. *Complex Syst.* **1989**, *3*, 493–530.
48. Schaffer, J.D. *Some Experiments in Machine Learning Using Vector Evaluated Genetic Algorithms (Artificial Intelligence, Optimization, Adaptation, Pattern Recognition)*; Vanderbilt University: Nashville, TN, USA, 1984.

49. Deb, K.; Pratap, A.; Agarwal, S.; Meyarivan, T. A fast and elitist multiobjective genetic algorithm: NSGA-II. *IEEE Trans. Evol. Comput.* **2002**, *6*, 182–197. [[CrossRef](#)]
50. Mondal, S.; Bhattacharya, A.; Nee Dey, S.H. Multi-objective economic emission load dispatch solution using gravitational search algorithm and considering wind power penetration. *Int. J. Electr. Power Energy Syst.* **2013**, *44*, 282–292. [[CrossRef](#)]
51. While, L.; Hingston, P.; Barone, L.; Huband, S. A faster algorithm for calculating hypervolume. *IEEE Trans. Evol. Comput.* **2006**, *10*, 29–38. [[CrossRef](#)]
52. Bringmann, K.; Friedrich, T. Approximation quality of the hypervolume indicator. *Artif. Intell.* **2013**, *195*, 265–290. [[CrossRef](#)]
53. Gazafroudi, A.S.; Shafie-khah, M.; Heydarian-Forushani, E.; Hajizadeh, A.; Heidari, A.; Corchado, J.M.; Catalão, J.P.S. Two-stage stochastic model for the price-based domestic energy management problem. *Int. J. Electr. Power Energy Syst.* **2019**, *112*, 404–416. [[CrossRef](#)]

Disclaimer/Publisher’s Note: The statements, opinions and data contained in all publications are solely those of the individual author(s) and contributor(s) and not of MDPI and/or the editor(s). MDPI and/or the editor(s) disclaim responsibility for any injury to people or property resulting from any ideas, methods, instructions or products referred to in the content.